15

Molecular spectroscopy 3: magnetic resonance

One of the most widely used spectroscopic procedures in chemistry makes use of the classical concept of resonance. The chapter begins with an account of conventional nuclear magnetic resonance, which shows how the resonance frequency of a magnetic nucleus is affected by its electronic environment and the presence of magnetic nuclei in its vicinity. Then we turn to the modern versions of NMR, which are based on the use of pulses of electromagnetic radiation and the processing of the resulting signal by Fourier transform techniques. The experimental techniques for electron paramagnetic resonance resemble those used in the early days of NMR. The information obtained is very useful for the determination of the properties of species with unpaired electrons.

When two pendulums share a slightly flexible support and one is set in motion, the other is forced into oscillation by the motion of the common axle. As a result, energy flows between the two pendulums. The energy transfer occurs most efficiently when the frequencies of the two pendulums are identical. The condition of strong effective coupling when the frequencies of two oscillators are identical is called **resonance**. Resonance is the basis of a number of everyday phenomena, including the response of radios to the weak oscillations of the electromagnetic field generated by a distant transmitter. In this chapter we explore some spectroscopic applications that, as originally developed (and in some cases still), depend on matching a set of energy levels to a source of monochromatic radiation and observing the strong absorption that occurs at resonance.

The effect of magnetic fields on electrons and nuclei

The Stern–Gerlach experiment (Section 9.8) provided evidence for electron spin. It turns out that many nuclei also possess spin angular momentum. Orbital and spin angular momenta give rise to magnetic moments, and to say that electrons and nuclei have magnetic moments means that, to some extent, they behave like small bar magnets. First, we establish how the energies of electrons and nuclei depend on the strength of an external field. Then we see how to use this dependence to study the structure and dynamics of complex molecules.

15.1 The energies of electrons in magnetic fields

Classically, the energy of a magnetic moment $\boldsymbol{\mu}$ in a magnetic field $\mathcal{B}$ is equal to the scalar product

The effect of magnetic fields on electrons and nuclei

15.1 The energies of electrons in magnetic fields
15.2 The energies of nuclei in magnetic fields
15.3 Magnetic resonance spectroscopy

Nuclear magnetic resonance

15.4 The NMR spectrometer
15.5 The chemical shift
15.6 The fine structure
15.7 Conformational conversion and exchange processes

Pulse techniques in NMR

15.8 The magnetization vector
15.9 Spin relaxation
I15.1 Impact on medicine: Magnetic resonance imaging
15.10 Spin decoupling
15.11 The nuclear Overhauser effect
15.12 Two-dimensional NMR
15.13 Solid-state NMR

Electron paramagnetic resonance

15.14 The EPR spectrometer
15.15 The *g*-value
15.16 Hyperfine structure
I15.2 Impact on biochemistry: Spin probes

Checklist of key ideas
Further reading
Further information 15.1: Fourier transformation of the FID curve
Discussion questions
Exercises
Problems

Comment 15.1
More formally, $\mathcal{B}$ is the magnetic induction and is measured in tesla, T; $1\ \mathrm{T} = 1\ \mathrm{kg\ s^{-2}\ A^{-1}}$. The (non-SI) unit gauss, G, is also occasionally used: $1\ \mathrm{T} = 10^4\ \mathrm{G}$.

Comment 15.2
The scalar product (or 'dot product') of two vectors $\boldsymbol{a}$ and $\boldsymbol{b}$ is given by $\boldsymbol{a}\cdot\boldsymbol{b} = ab\cos\theta$, where a and b are the magnitudes of $\boldsymbol{a}$ and $\boldsymbol{b}$, respectively, and θ is the angle between them.

$$E = -\boldsymbol{\mu}\cdot\boldsymbol{\mathcal{B}} \tag{15.1}$$

Quantum mechanically, we write the hamiltonian as

$$\hat{H} = -\hat{\boldsymbol{\mu}}\cdot\boldsymbol{\mathcal{B}} \tag{15.2}$$

To write an expression for $\hat{\boldsymbol{\mu}}$, we recall from Section 9.8 that the magnetic moment is proportional to the angular momentum. For an electron possessing orbital angular momentum we write

$$\hat{\boldsymbol{\mu}} = \gamma_e\hat{\boldsymbol{l}} \qquad \text{and} \qquad \hat{H} = -\gamma_e\boldsymbol{\mathcal{B}}\cdot\hat{\boldsymbol{l}} \tag{15.3}$$

where $\hat{\boldsymbol{l}}$ is the orbital angular momentum operator and

$$\gamma_e = -\frac{e}{2m_e} \tag{15.4}$$

γ_e is called the **magnetogyric ratio** of the electron: The negative sign (arising from the sign of the electron's charge) shows that the orbital moment is antiparallel to its orbital angular momentum (as was depicted in Fig 10.26).

For a magnetic field $\mathcal{B}_0$ along the z-direction, eqn 15.3 becomes

$$\hat{\mu}_z = \gamma_e\hat{l}_z \qquad \text{and} \qquad \hat{H} = -\gamma_e\mathcal{B}_0\hat{l}_z = -\hat{\mu}_z\mathcal{B}_0 \tag{15.5a}$$

Because the eigenvalues of the operator $\hat{\boldsymbol{l}}_z$ are $m_l\hbar$, the z-component of the orbital magnetic moment and the energy of interaction are, respectively,

$$\mu_z = \gamma_e m_l\hbar \qquad \text{and} \qquad E = -\gamma_e m_l\hbar\mathcal{B}_0 = m_l\mu_B\mathcal{B}_0 \tag{15.5b}$$

where the **Bohr magneton**, μ_B, is

$$\mu_B = -\gamma_e\hbar = \frac{e\hbar}{2m_e} = 9.724\times10^{-24}\ \mathrm{J\ T^{-1}} \tag{15.6}$$

The Bohr magneton is often regarded as the fundamental quantum of magnetic moment.

The spin magnetic moment of an electron, which has a spin quantum number $s = \frac{1}{2}$ (Section 9.8), is also proportional to its spin angular momentum. However, instead of eqn 15.3, the spin magnetic moment and hamiltonian operators are, respectively,

$$\hat{\boldsymbol{\mu}} = g_e\gamma_e\hat{\boldsymbol{s}} \qquad \text{and} \qquad \hat{H} = -g_e\gamma_e\boldsymbol{\mathcal{B}}\cdot\hat{\boldsymbol{s}} \tag{15.7}$$

where $\hat{\boldsymbol{s}}$ is the spin angular momentum operator and the extra factor g_e is called the ***g*-value** of the electron: $g_e = 2.002\,319\ldots$. The g-value arises from relativistic effects and from interactions of the electron with the electromagnetic fluctuations of the vacuum that surrounds the electron. For a magnetic field $\mathcal{B}_0$ in the z-direction,

$$\hat{\mu}_z = g_e\gamma_e\hat{s}_z \qquad \text{and} \qquad \hat{H} = -g_e\gamma_e\mathcal{B}_0\hat{s}_z \tag{15.8a}$$

Because the eigenvalues of the operator $\hat{s}_z$ are $m_s\hbar$ with $m_s = +\frac{1}{2}(\alpha)$ and $m_s = -\frac{1}{2}(\beta)$, it follows that the energies of an electron spin in a magnetic field are

$$\mu_z = g_e\gamma_e m_s\hbar \qquad \text{and} \qquad E_{m_s} = -g_e\gamma_e m_s\hbar\mathcal{B}_0 = g_e\mu_B m_s\mathcal{B}_0 \tag{15.8b}$$

with $m_s = \pm\frac{1}{2}$.

In the absence of a magnetic field, the states with different values of m_l and m_s are degenerate. When a field is present, the degeneracy is removed: the state with $m_s = +\frac{1}{2}$ moves up in energy by $\frac{1}{2}g_e\mu_B\mathcal{B}_0$ and the state with $m_s = -\frac{1}{2}$ moves down by $\frac{1}{2}g_e\mu_B\mathcal{B}_0$. The different energies arising from an interaction with an external field are sometimes represented on the vector model by picturing the vectors as **precessing**, or sweeping

Table 15.1 Nuclear constitution and the nuclear spin quantum number*

Number of protons	Number of neutrons	I
even	even	0
odd	odd	integer (1, 2, 3, . . .)
even	odd	half-integer ($\frac{1}{2}, \frac{3}{2}, \frac{5}{2}, \ldots$)
odd	even	half-integer ($\frac{1}{2}, \frac{3}{2}, \frac{5}{2}, \ldots$)

* The spin of a nucleus may be different if it is in an excited state; throughout this chapter we deal only with the ground state of nuclei.

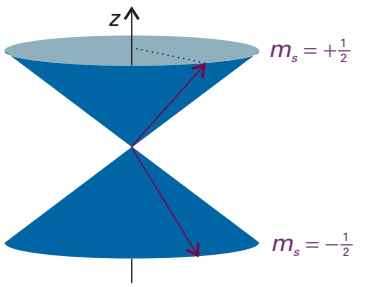

Fig. 15.1 The interactions between the m_s states of an electron and an external magnetic field may be visualized as the precession of the vectors representing the angular momentum.

round their cones (Fig. 15.1), with the rate of precession equal to the **Larmor frequency**, ν_L:

$$\nu_L = \frac{\gamma_e \mathcal{B}_0}{2\pi} \tag{15.9}$$

Equation 15.9 shows that the Larmor frequency increases with the strength of the magnetic field. For a field of 1 T, the Larmor frequency is 30 GHz.

15.2 The energies of nuclei in magnetic fields

The spin quantum number, I, of a nucleus is a fixed characteristic property of a nucleus and is either an integer or a half-integer (Table 15.1). A nucleus with spin quantum number I has the following properties:

1. An angular momentum of magnitude $\{I(I+1)\}^{1/2}\hbar$.
2. A component of angular momentum $m_I\hbar$ on a specified axis ('the z-axis'), where $m_I = I, I-1, \ldots, -I$.
3. If $I > 0$, a magnetic moment with a constant magnitude and an orientation that is determined by the value of m_I.

According to the second property, the spin, and hence the magnetic moment, of the nucleus may lie in $2I + 1$ different orientations relative to an axis. A proton has $I = \frac{1}{2}$ and its spin may adopt either of two orientations; a ^{14}N nucleus has $I = 1$ and its spin may adopt any of three orientations; both ^{12}C and ^{16}O have $I = 0$ and hence zero magnetic moment.

The energy of interaction between a nucleus with a magnetic moment $\boldsymbol{\mu}$ and an external magnetic field $\boldsymbol{\mathcal{B}}$ may be calculated by using operators analogous to those of eqn 15.3:

$$\hat{\boldsymbol{\mu}} = \gamma\hat{\mathbf{I}} \qquad \text{and} \qquad H = -\gamma\boldsymbol{\mathcal{B}}\cdot\hat{\mathbf{I}} \tag{15.10a}$$

where γ is the magnetogyric ratio of the specified nucleus, an empirically determined characteristic arising from the internal structure of the nucleus (Table 15.2). The corresponding energies are

$$E_{m_I} = -\mu_z\mathcal{B}_0 = -\gamma\hbar\mathcal{B}_0 m_I \tag{15.10b}$$

As for electrons, the nuclear spin may be pictured as precessing around the direction of the applied field at a rate proportional to the applied field. For protons, a field of 1 T corresponds to a Larmor frequency (eqn 15.9, with γ_e replaced by γ) of about 40 MHz.

Synoptic table 15.2* Nuclear spin properties

Nuclide	Natural abundance/%	Spin I	g-factor, g_I	Magnetogyric ratio, $\gamma/(10^7\ \mathrm{T^{-1}\ s^{-1}})$	NMR frequency at 1 T, ν/MHz
^{1}n		$\frac{1}{2}$	−3.826	−18.32	29.165
^{1}H	99.98	$\frac{1}{2}$	5.586	26.75	42.577
^{2}H	0.02	1	0.857	4.10	6.536
^{13}C	1.11	$\frac{1}{2}$	1.405	6.73	10.705
^{14}N	99.64	1	0.404	1.93	3.076

* More values are given in the *Data section*.

The magnetic moment of a nucleus is sometimes expressed in terms of the **nuclear *g*-factor**, g_I, a characteristic of the nucleus, and the **nuclear magneton**, μ_N, a quantity independent of the nucleus, by using

$$\gamma\hbar = g_I\mu_N \qquad \mu_N = \frac{e\hbar}{2m_p} = 5.051\times10^{-27}\ \mathrm{J\ T^{-1}} \qquad [15.11]$$

where m_p is the mass of the proton. Nuclear g-factors vary between −6 and +6 (see Table 15.2): positive values of g_I and γ denote a magnetic moment that is parallel to the spin; negative values indicate that the magnetic moment and spin are antiparallel. For the remainder of this chapter we shall assume that γ is positive, as is the case for the majority of nuclei. In such cases, the states with negative values of m_I lie above states with positive values of m_I. The nuclear magneton is about 2000 times smaller than the Bohr magneton, so nuclear magnetic moments—and consequently the energies of interaction with magnetic fields—are about 2000 times weaker than the electron spin magnetic moment.

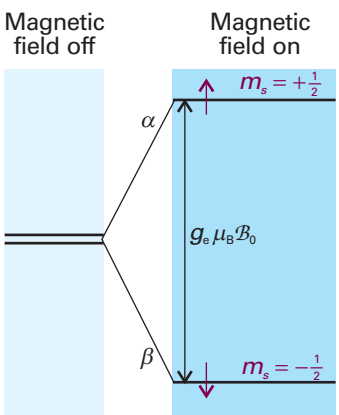

Fig. 15.2 Electron spin levels in a magnetic field. Note that the β state is lower in energy than the α state (because the magnetogyric ratio of an electron is negative). Resonance is achieved when the frequency of the incident radiation matches the frequency corresponding to the energy separation.

15.3 Magnetic resonance spectroscopy

In its original form, the magnetic resonance experiment is the resonant absorption of radiation by nuclei or unpaired electrons in a magnetic field. From eqn 15.8b, the separation between the $m_s = -\frac{1}{2}$ and $m_s = +\frac{1}{2}$ levels of an electron spin in a magnetic field $\mathcal{B}_0$ is

$$\Delta E = E_\alpha - E_\beta = g_e\mu_B\mathcal{B}_0 \qquad (15.12a)$$

If the sample is exposed to radiation of frequency ν, the energy separations come into resonance with the radiation when the frequency satisfies the **resonance condition** (Fig. 15.2):

$$h\nu = g_e\mu_B\mathcal{B}_0 \qquad (15.12b)$$

At resonance there is strong coupling between the electron spins and the radiation, and strong absorption occurs as the spins make the transition $\beta \rightarrow \alpha$. **Electron paramagnetic resonance** (EPR), or **electron spin resonance** (ESR), is the study of molecules and ions containing unpaired electrons by observing the magnetic fields at which they come into resonance with monochromatic radiation. Magnetic fields of about 0.3 T (the value used in most commercial EPR spectrometers) correspond to resonance with an electromagnetic field of frequency 10 GHz (10^{10} Hz) and wavelength 3 cm. Because 3 cm radiation falls in the microwave region of the electromagnetic spectrum, EPR is a microwave technique.

The energy separation between the $m_I = +\frac{1}{2}$ ($\uparrow$ or α) and the $m_I = -\frac{1}{2}$ ($\downarrow$ or β) states of **spin-$\frac{1}{2}$ nuclei**, which are nuclei with $I = \frac{1}{2}$, is

$$\Delta E = E_\beta - E_\alpha = \tfrac{1}{2}\gamma\hbar\mathcal{B}_0 - (-\tfrac{1}{2}\gamma\hbar\mathcal{B}_0) = \gamma\hbar\mathcal{B}_0 \qquad (15.13a)$$

and resonant absorption occurs when the resonance condition (Fig. 15.3)

$$h\nu = \gamma\hbar\mathcal{B}_0 \qquad (15.13b)$$

is fulfilled. Because $\gamma\hbar\mathcal{B}_0/h$ is the Larmor frequency of the nucleus, this resonance occurs when the frequency of the electromagnetic field matches the Larmor frequency ($\nu = \nu_L$). In its simplest form, **nuclear magnetic resonance** (NMR) is the study of the properties of molecules containing magnetic nuclei by applying a magnetic field and observing the frequency of the resonant electromagnetic field. Larmor frequencies of nuclei at the fields normally employed (about 12 T) typically lie in the radiofrequency region of the electromagnetic spectrum (close to 500 MHz), so NMR is a radiofrequency technique.

For much of this chapter we consider spin-$\frac{1}{2}$ nuclei, but NMR is applicable to nuclei with any non-zero spin. As well as protons, which are the most common nuclei studied by NMR, spin-$\frac{1}{2}$ nuclei include ^{13}C, ^{19}F, and ^{31}P.

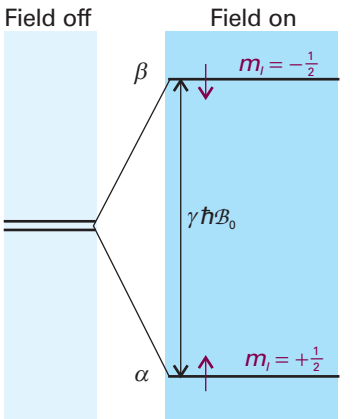

Fig. 15.3 The nuclear spin energy levels of a spin-$\frac{1}{2}$ nucleus with positive magnetogyric ratio (for example, ^1H or ^{13}C) in a magnetic field. Resonance occurs when the energy separation of the levels matches the energy of the photons in the electromagnetic field.

Nuclear magnetic resonance

Although the NMR technique is simple in concept, NMR spectra can be highly complex. However, they have proved invaluable in chemistry, for they reveal so much structural information. A magnetic nucleus is a very sensitive, non-invasive probe of the surrounding electronic structure.

15.4 The NMR spectrometer

An NMR spectrometer consists of the appropriate sources of radiofrequency electromagnetic radiation and a magnet that can produce a uniform, intense field. In simple instruments, the magnetic field is provided by a permanent magnet. For serious work, a **superconducting magnet** capable of producing fields of the order of 10 T and more is used (Fig. 15.4). The sample is placed in the cylindrically wound magnet. In some cases the sample is rotated rapidly to average out magnetic inhomogeneities. However, sample spinning can lead to irreproducible results, and is often avoided. Although a superconducting magnet operates at the temperature of liquid helium (4 K), the sample itself is normally at room temperature.

The intensity of an NMR transition depends on a number of factors. We show in the following *Justification* that

$$\text{Intensity} \propto (N_\alpha - N_\beta)\mathcal{B}_0 \qquad (15.14a)$$

where

$$N_\alpha - N_\beta \approx \frac{N\gamma\hbar\mathcal{B}_0}{2kT} \qquad (15.14b)$$

with N the total number of spins ($N = N_\alpha + N_\beta$). It follows that decreasing the temperature increases the intensity by increasing the population difference. By combining these two equations we see that the intensity is proportional to $\mathcal{B}_0^2$, so NMR transitions can be enhanced significantly by increasing the strength of the applied magnetic field. We shall also see (Section 15.6) that the use of high magnetic fields simplifies the

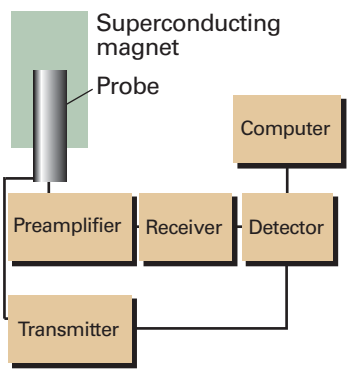

Fig. 15.4 The layout of a typical NMR spectrometer. The link from the transmitter to the detector indicates that the high frequency of the transmitter is subtracted from the high frequency received signal to give a low frequency signal for processing.

appearance of spectra and so allows them to be interpreted more readily. We also conclude that absorptions of nuclei with large magnetogyric ratios (^{1}H, for instance) are more intense than those with small magnetogyric ratios (^{13}C, for instance)

Justification 15.1 *Intensities in NMR spectra*

From the general considerations of transition intensities in Section 13.2, we know that the rate of absorption of electromagnetic radiation is proportional to the population of the lower energy state (N_α in the case of a proton NMR transition) and the rate of stimulated emission is proportional to the population of the upper state (N_β). At the low frequencies typical of magnetic resonance, we can neglect spontaneous emission as it is very slow. Therefore, the net rate of absorption is proportional to the difference in populations, and we can write

$$\text{Rate of absorption} \propto N_\alpha - N_\beta$$

The intensity of absorption, the rate at which energy is absorbed, is proportional to the product of the rate of absorption (the rate at which photons are absorbed) and the energy of each photon, and the latter is proportional to the frequency ν of the incident radiation (through $E = h\nu$). At resonance, this frequency is proportional to the applied magnetic field (through $\nu = \nu_L = \gamma' \mathcal{B}_0/2\pi$), so we can write

$$\text{Intensity of absorption} \propto (N_\alpha - N_\beta)\mathcal{B}_0$$

as in eqn 15.14a. To write an expression for the population difference, we use the Boltzmann distribution (*Molecular interpretation* 3.1) to write the ratio of populations as

$$\frac{N_\beta}{N_\alpha} = e^{-\Delta E/kT} \approx 1 - \frac{\Delta E}{kT} = 1 - \frac{\gamma' \mathcal{B}_0}{kT}$$

Comment 15.3
The expansion of an exponential function used here is $e^{-x} = 1 - x + \frac{1}{2}x^2 - \ldots$. If $x \ll 1$, then $e^{-x} \approx 1 - x$.

where $\Delta E = E_\beta - E_\alpha$. The expansion of the exponential term is appropriate for $\Delta E \ll kT$, a condition usually met for nuclear spins. It follows after rearrangement that

$$\frac{N_\alpha - N_\beta}{N_\alpha + N_\beta} = \frac{N_\alpha(1 - N_\beta/N_\alpha)}{N_\alpha(1 + N_\beta/N_\alpha)} = \frac{1 - N_\beta/N_\alpha}{1 + N_\beta/N_\alpha}$$

$$\approx \frac{1 - (1 - \gamma\hbar\mathcal{B}_0/kT)}{1 + (1 - \gamma\hbar\mathcal{B}_0/kT)} \approx \frac{\gamma\hbar\mathcal{B}_0/kT}{2}$$

Then, with $N_\alpha + N_\beta = N$, the total number of spins, we obtain eqn 15.14b.

15.5 The chemical shift

Nuclear magnetic moments interact with the *local* magnetic field. The local field may differ from the applied field because the latter induces electronic orbital angular momentum (that is, the circulation of electronic currents) which gives rise to a small additional magnetic field $\delta\mathcal{B}$ at the nuclei. This additional field is proportional to the applied field, and it is conventional to write

$$\delta\mathcal{B} = -\sigma\mathcal{B}_0 \qquad [15.15]$$

where the dimensionless quantity σ is called the **shielding constant** of the nucleus (σ is usually positive but may be negative). The ability of the applied field to induce an electronic current in the molecule, and hence affect the strength of the resulting local magnetic field experienced by the nucleus, depends on the details of the electronic structure near the magnetic nucleus of interest, so nuclei in different chemical groups have

different shielding constants. The calculation of reliable values of the shielding constant is very difficult, but trends in it are quite well understood and we concentrate on them.

(a) The δ scale of chemical shifts

Because the total local field is

$$\mathcal{B}_{\text{loc}} = \mathcal{B}_0 + \delta\mathcal{B} = (1-\sigma)\mathcal{B}_0 \tag{15.16}$$

the nuclear Larmor frequency is

$$\nu_{\text{L}} = \frac{\gamma\mathcal{B}_{\text{loc}}}{2\pi} = (1-\sigma)\frac{\gamma\mathcal{B}_0}{2\pi} \tag{15.17}$$

This frequency is different for nuclei in different environments. Hence, different nuclei, even of the same element, come into resonance at different frequencies.

It is conventional to express the resonance frequencies in terms of an empirical quantity called the **chemical shift**, which is related to the difference between the resonance frequency, ν, of the nucleus in question and that of a reference standard, ν°:

$$\delta = \frac{\nu - \nu^\circ}{\nu^\circ} \times 10^6 \tag{15.18}$$

The standard for protons is the proton resonance in tetramethylsilane ($Si(CH_3)_4$, commonly referred to as TMS), which bristles with protons and dissolves without reaction in many liquids. Other references are used for other nuclei. For ^{13}C, the reference frequency is the ^{13}C resonance in TMS; for ^{31}P it is the ^{31}P resonance in 85 per cent $H_3PO_4(aq)$. The advantage of the δ-scale is that shifts reported on it are independent of the applied field (because both numerator and denominator are proportional to the applied field).

Illustration 15.1 *Using the chemical shift*

From eqn 15.18,

$$\nu - \nu^\circ = \nu^\circ\delta \times 10^{-6}$$

A nucleus with $\delta = 1.00$ in a spectrometer operating at 500 MHz will have a shift relative to the reference equal to

$$\nu - \nu^\circ = (500\ \text{MHz}) \times 1.00 \times 10^{-6} = 500\ \text{Hz}$$

In a spectrometer operating at 100 MHz, the shift relative to the reference would be only 100 Hz.

A note on good practice In much of the literature, chemical shifts are reported in 'parts per million', ppm, in recognition of the factor of 10^6 in the definition. This practice is unnecessary.

The relation between δ and σ is obtained by substituting eqn 15.17 into eqn 15.18:

$$\delta = \frac{(1-\sigma)\mathcal{B}_0 - (1-\sigma^\circ)\mathcal{B}_0}{(1-\sigma^\circ)\mathcal{B}_0} \times 10^6 = \frac{\sigma^\circ - \sigma}{1-\sigma^\circ} \times 10^6 \approx (\sigma^\circ - \sigma) \times 10^6 \tag{15.19}$$

As the shielding, σ, gets smaller, δ *increases*. Therefore, we speak of nuclei with large chemical shift as being strongly **deshielded**. Some typical chemical shifts are given in Fig. 15.5. As can be seen from the illustration, the nuclei of different elements have

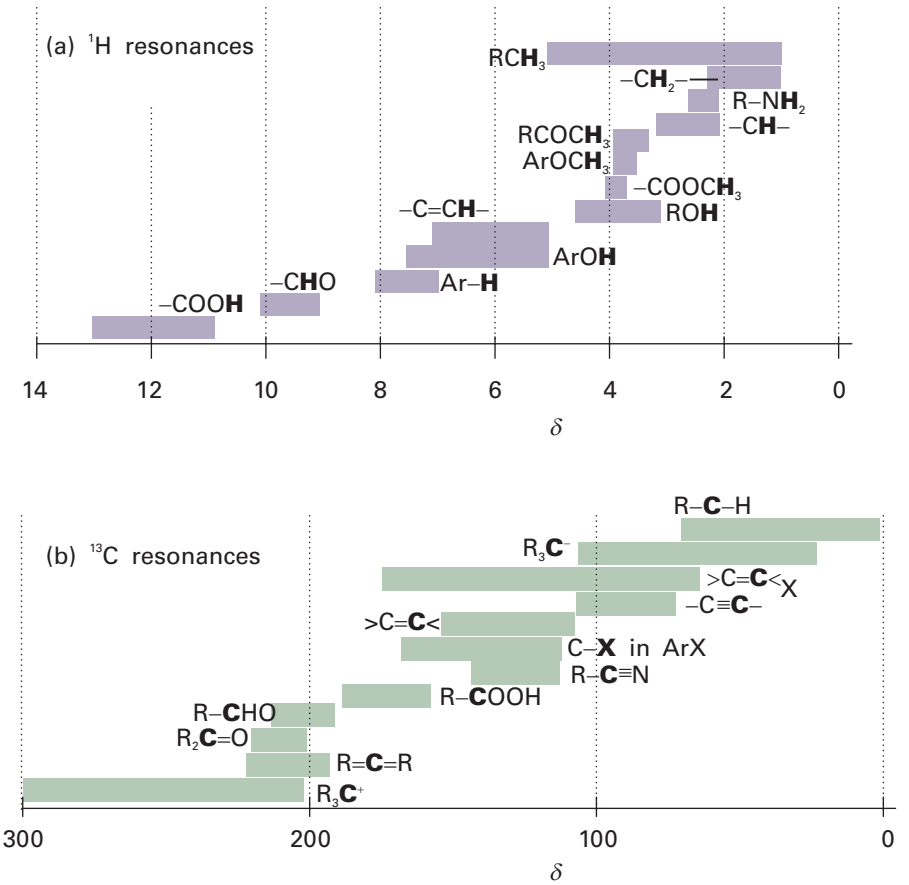

Fig. 15.5 The range of typical chemical shifts for (a) ^{1}H resonances and (b) ^{13}C resonances.

very different ranges of chemical shifts. The ranges exhibit the variety of electronic environments of the nuclei in molecules: the heavier the element, the greater the number of electrons around the nucleus and hence the greater the range of shieldings.

By convention, NMR spectra are plotted with δ increasing from right to left. Consequently, in a given applied magnetic field the Larmor frequency also increases from right to left. In the original continuous wave (CW) spectrometers, in which the radiofrequency was held constant and the magnetic field varied (a 'field sweep experiment'), the spectrum was displayed with the applied magnetic field increasing from left to right: a nucleus with a small chemical shift experiences a relatively low local magnetic field, so it needs a higher applied magnetic field to bring it into resonance with the radiofrequency field. Consequently, the right-hand (low chemical shift) end of the spectrum became known as the 'high field end' of the spectrum.

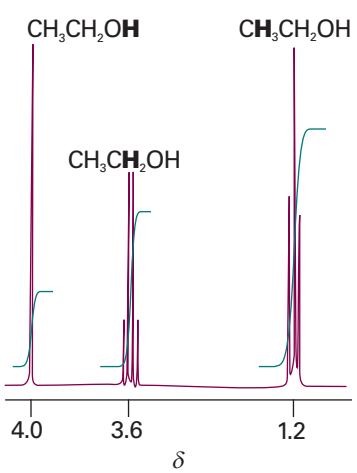

Fig. 15.6 The ^{1}H-NMR spectrum of ethanol. The bold letters denote the protons giving rise to the resonance peak, and the step-like curve is the integrated signal.

(b) Resonance of different groups of nuclei

The existence of a chemical shift explains the general features of the spectrum of ethanol shown in Fig.15.6. The CH_3 protons form one group of nuclei with $\delta \approx 1$. The two CH_2 protons are in a different part of the molecule, experience a different local magnetic field, and resonate at $\delta \approx 3$. Finally, the OH proton is in another environment, and has a chemical shift of $\delta \approx 4$. The increasing value of δ (that is, the decrease in shielding) is consistent with the electron-withdrawing power of the O atom: it reduces the electron density of the OH proton most, and that proton is strongly deshielded. It reduces the electron density of the distant methyl protons least, and those nuclei are least deshielded.

The relative intensities of the signals (the areas under the absorption lines) can be used to help distinguish which group of lines corresponds to which chemical group. The determination of the area under an absorption line is referred to as the **integration** of the signal (just as any area under a curve may be determined by mathematical integration). Spectrometers can integrate the absorption automatically (as indicated in Fig. 15.6). In ethanol the group intensities are in the ratio 3:2:1 because there are three CH_3 protons, two CH_2 protons, and one OH proton in each molecule. Counting the number of magnetic nuclei as well as noting their chemical shifts helps to identify a compound present in a sample.

(c) The origin of shielding constants

The calculation of shielding constants is difficult, even for small molecules, for it requires detailed information about the distribution of electron density in the ground and excited states and the excitation energies of the molecule. Nevertheless, considerable success has been achieved with the calculation for diatomic molecules and small molecules such as H_2O and CH_4 and even large molecules, such as proteins, are within the scope of some types of calculation. Nevertheless, it is easier to understand the different contributions to chemical shifts by studying the large body of empirical information now available for large molecules.

The empirical approach supposes that the observed shielding constant is the sum of three contributions:

$$\sigma = \sigma(\text{local}) + \sigma(\text{neighbour}) + \sigma(\text{solvent}) \tag{15.20}$$

The **local contribution**, σ(local), is essentially the contribution of the electrons of the atom that contains the nucleus in question. The **neighbouring group contribution**, σ(neighbour), is the contribution from the groups of atoms that form the rest of the molecule. The **solvent contribution**, σ(solvent), is the contribution from the solvent molecules.

(d) The local contribution

It is convenient to regard the local contribution to the shielding constant as the sum of a **diamagnetic contribution**, σ_d, and a **paramagnetic contribution**, σ_p:

$$\sigma(\text{local}) = \sigma_d + \sigma_p \tag{15.21}$$

A diamagnetic contribution to σ(local) opposes the applied magnetic field and shields the nucleus in question. A paramagnetic contribution to σ(local) reinforces the applied magnetic field and deshields the nucleus in question. Therefore, $\sigma_d > 0$ and $\sigma_p < 0$. The total local contribution is positive if the diamagnetic contribution dominates, and is negative if the paramagnetic contribution dominates.

The diamagnetic contribution arises from the ability of the applied field to generate a circulation of charge in the ground-state electron distribution of the atom. The circulation generates a magnetic field that opposes the applied field and hence shields the nucleus. The magnitude of σ_d depends on the electron density close to the nucleus and can be calculated from the **Lamb formula** (see *Further reading* for a derivation):

$$\sigma_d = \frac{e^2\mu_0}{12\pi m_e}\left\langle \frac{1}{r} \right\rangle \tag{15.22}$$

where μ_0 is the vacuum permeability (a fundamental constant, see inside the front cover) and r is the electron–nucleus distance.

Illustration 15.2 *Calculating the diamagnetic contribution to the chemical shift of a proton*

To calculate σ_d for the proton in a free H atom, we need to calculate the expectation value of $1/r$ for a hydrogen 1*s* orbital. Wavefunctions are given in Table 10.1, and a useful integral is given in Example 8.7. Because $d\tau = r^2 dr \sin\theta\, d\theta d\phi$, we can write

$$\left\langle \frac{1}{r} \right\rangle = \int \frac{\psi^*\psi}{r} d\tau = \frac{1}{\pi a_0^3} \int_0^{2\pi} d\phi \int_0^{\pi} \sin\theta d\theta \int_0^{\infty} r e^{-2r/a_0} dr = \frac{4}{a_0^3} \int_0^{\infty} r e^{-2r/a_0} dr = \frac{1}{a_0}$$

Therefore,

$$\sigma_d = \frac{e^2 \mu_0}{12\pi m_e a_0}$$

With the values of the fundamental constants inside the front cover, this expression evaluates to 1.78×10^{-5}.

The diamagnetic contribution is the only contribution in closed-shell free atoms. It is also the only contribution to the local shielding for electron distributions that have spherical or cylindrical symmetry. Thus, it is the only contribution to the local shielding from inner cores of atoms, for cores remain spherical even though the atom may be a component of a molecule and its valence electron distribution highly distorted. The diamagnetic contribution is broadly proportional to the electron density of the atom containing the nucleus of interest. It follows that the shielding is decreased if the electron density on the atom is reduced by the influence of an electronegative atom nearby. That reduction in shielding translates into an increase in deshielding, and hence to an increase in the chemical shift δ as the electronegativity of a neighbouring atom increases (Fig. 15.7). That is, as the electronegativity increases, δ decreases.

The local paramagnetic contribution, σ_p, arises from the ability of the applied field to force electrons to circulate through the molecule by making use of orbitals that are unoccupied in the ground state. It is zero in free atoms and around the axes of linear molecules (such as ethyne, HC≡CH) where the electrons can circulate freely and a field applied along the internuclear axis is unable to force them into other orbitals. We can expect large paramagnetic contributions from small atoms in molecules with low-lying excited states. In fact, the paramagnetic contribution is the dominant local contribution for atoms other than hydrogen.

(e) Neighbouring group contributions

The neighbouring group contribution arises from the currents induced in nearby groups of atoms. Consider the influence of the neighbouring group X on the proton H in a molecule such as H—X. The applied field generates currents in the electron distribution of X and gives rise to an induced magnetic moment proportional to the applied field; the constant of proportionality is the magnetic susceptibility, χ (chi), of the group X. The proton H is affected by this induced magnetic moment in two ways. First, the strength of the additional magnetic field the proton experiences is inversely proportional to the cube of the distance r between H and X. Second, the field at H depends on the anisotropy of the magnetic susceptibility of X, the variation of χ with the angle that X makes to the applied field. We assume that the magnetic susceptibility of X has two components, $\chi_\parallel$ and $\chi_\perp$, which are parallel and perpendicular to the axis of symmetry of X, respectively. The axis of symmetry of X makes an angle θ to the

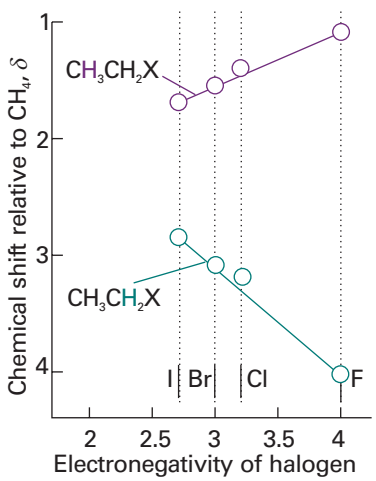

Fig. 15.7 The variation of chemical shielding with electronegativity. The shifts for the methylene protons agree with the trend expected with increasing electronegativity. However, to emphasize that chemical shifts are subtle phenomena, notice that the trend for the methyl protons is opposite to that expected. For these protons another contribution (the magnetic anisotropy of C—H and C—X bonds) is dominant.

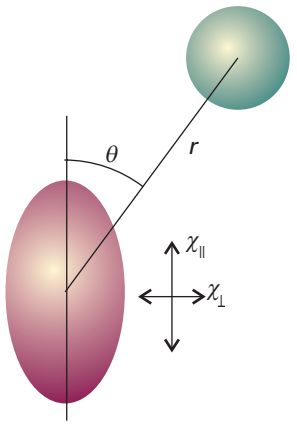

1

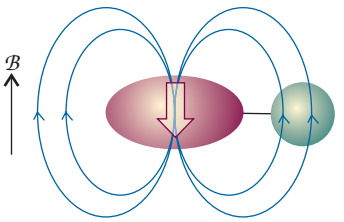

2

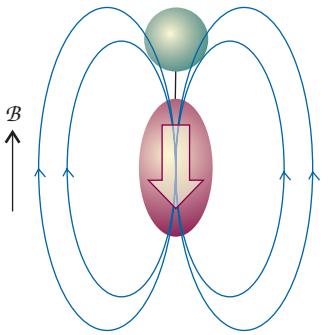

3

vector connecting X to H (**1**, where X is represented by the ellipse and H is represented by the circle).

To examine the effect of anisotropy of the magnetic susceptibility of X on the shielding constant, consider the case $\theta = 0$ for a molecule H—X that is free to tumble (**2** and **3**). Some of the time the H—X axis will be perpendicular to the applied field and then only $\chi_\perp$ will contribute to the induced magnetic moment that shields X from the applied field. The result is deshielding of the proton H, or $\sigma(\text{neighbour}) < 0$ (**2**). When the applied field is parallel to the H—X axis, only $\chi_\parallel$ contributes to the induced magnetic moment at X. The result is shielding of the proton H (**3**). We conclude that, as the molecule tumbles and the H—X axis takes all possible angles with respect to the applied field, the effects of anisotropic magnetic susceptibility do not average to zero because $\chi_\parallel \neq \chi_\perp$.

Self-test 15.1 For a tumbling H—X molecule, show that when $\theta = 90°$: (a) contributions from the $\chi_\perp$ component lead to shielding of H, or $\sigma(\text{neighbour}) > 0$, and (b) contributions from the $\chi_\parallel$ component lead to deshielding of H, or $\sigma(\text{neighbour}) < 0$. Comparison between the $\theta = 0$ and $\theta = 90°$ cases shows that the patterns of shielding and deshielding by neighbouring groups depend not only on differences between $\chi_\parallel$ and $\chi_\perp$, but also the angle θ.

[Draw diagrams similar to **2** and **3** where the $\chi_\perp$ component is parallel to the H—X axis and then analyse the problem as above.]

To a good approximation, the shielding constant $\sigma(\text{neighbour})$ depends on the distance r, the difference $\chi_\parallel - \chi_\perp$, as (see *Further reading* for a derivation)

$$\sigma(\text{neighbour}) \propto (\chi_\parallel - \chi_\perp)\left(\frac{1 - 3\cos^2\theta}{r^3}\right) \qquad (15.23)$$

where $\chi_\parallel$ and $\chi_\perp$ are both negative for a diamagnetic group X. Equation 15.23 shows that the neighbouring group contribution may be positive or negative according to the relative magnitudes of the two magnetic susceptibilities and the relative orientation of the nucleus with respect to X. The latter effect is easy to anticipate: if $54.7° < \theta < 125.3°$, then $1 - 3\cos^2\theta$ is positive, but it is negative otherwise (Fig. 15.8).

A special case of a neighbouring group effect is found in aromatic compounds. The strong anisotropy of the magnetic susceptibility of the benzene ring is ascribed to the

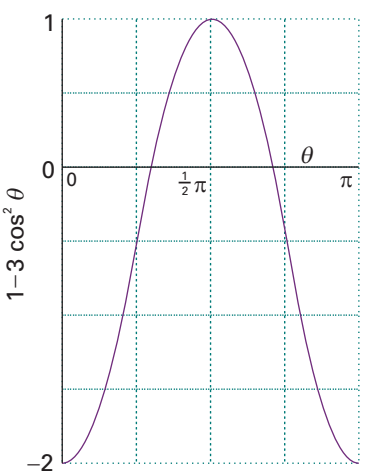

Fig. 15.8 The variation of the function $1 - 3\cos^2\theta$ with the angle θ.

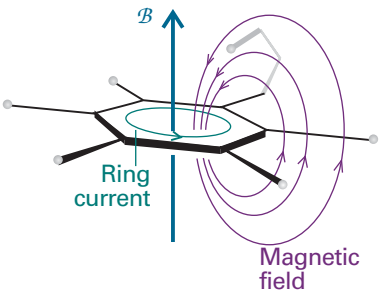

Fig. 15.9 The shielding and deshielding effects of the ring current induced in the benzene ring by the applied field. Protons attached to the ring are deshielded but a proton attached to a substituent that projects above the ring is shielded.

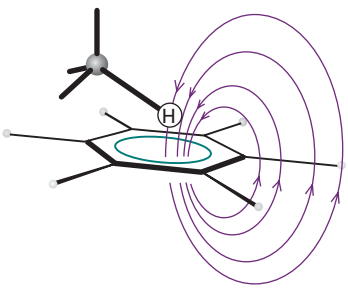

Fig. 15.10 An aromatic solvent (benzene here) can give rise to local currents that shield or deshield a proton in a solvent molecule. In this relative orientation of the solvent and solute, the proton on the solute molecule is shielded.

ability of the field to induce a **ring current**, a circulation of electrons around the ring, when it is applied perpendicular to the molecular plane. Protons in the plane are deshielded (Fig. 15.9), but any that happen to lie above or below the plane (as members of substituents of the ring) are shielded.

(f) The solvent contribution

A solvent can influence the local magnetic field experienced by a nucleus in a variety of ways. Some of these effects arise from specific interactions between the solute and the solvent (such as hydrogen-bond formation and other forms of Lewis acid–base complex formation). The anisotropy of the magnetic susceptibility of the solvent molecules, especially if they are aromatic, can also be the source of a local magnetic field. Moreover, if there are steric interactions that result in a loose but specific interaction between a solute molecule and a solvent molecule, then protons in the solute molecule may experience shielding or deshielding effects according to their location relative to the solvent molecule (Fig. 15.10). We shall see that the NMR spectra of species that contain protons with widely different chemical shifts are easier to interpret than those in which the shifts are similar, so the appropriate choice of solvent may help to simplify the appearance and interpretation of a spectrum.

15.6 The fine structure

The splitting of resonances into individual lines in Fig. 15.6 is called the **fine structure** of the spectrum. It arises because each magnetic nucleus may contribute to the local field experienced by the other nuclei and so modify their resonance frequencies. The strength of the interaction is expressed in terms of the **scalar coupling constant**, J, and reported in hertz (Hz). The scalar coupling constant is so called because the energy of interaction it describes is proportional to the scalar product of the two interacting spins: $E \propto \boldsymbol{I}_1 \cdot \boldsymbol{I}_2$. The constant of proportionality in this expression is $hJ/\hbar^2$, because each angular momentum is proportional to $\hbar$.

Spin coupling constants are independent of the strength of the applied field because they do not depend on the latter for their ability to generate local fields. If the resonance line of a particular nucleus is split by a certain amount by a second nucleus, then the resonance line of the second nucleus is split by the first to the same extent.

(a) The energy levels of coupled systems

It will be useful for later discussions to consider an NMR spectrum in terms of the energy levels of the nuclei and the transitions between them. In NMR, letters far apart in the alphabet (typically A and X) are used to indicate nuclei with very different chemical shifts; letters close together (such as A and B) are used for nuclei with similar chemical shifts. We shall consider first an AX system, a molecule that contains two spin-$\frac{1}{2}$ nuclei A and X with very different chemical shifts in the sense that the difference in chemical shift corresponds to a frequency that is large compared to their spin–spin coupling.

The energy level diagram for a single spin-$\frac{1}{2}$ nucleus and its single transition were shown in Fig. 15.3, and nothing more needs to be said. For a spin-$\frac{1}{2}$ AX system there are four spin states:

$$\alpha_A\alpha_X \qquad \alpha_A\beta_X \qquad \beta_A\alpha_X \quad \beta_A\beta_X$$

The energy depends on the orientation of the spins in the external magnetic field, and if spin–spin coupling is neglected

$$E = -\gamma\hbar(1-\sigma_A)\mathcal{B}m_A - \gamma\hbar(1-\sigma_X)\mathcal{B}m_X = -h\nu_A m_A - h\nu_X m_X \qquad (15.24)$$

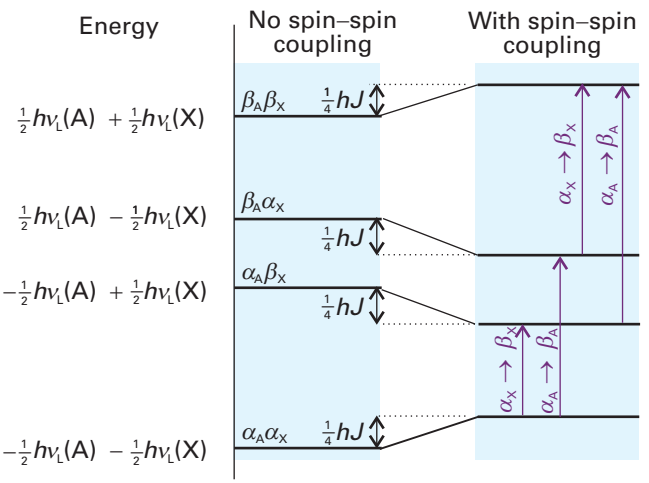

Fig. 15.11 The energy levels of an AX system. The four levels on the left are those of the two spins in the absence of spin–spin coupling. The four levels on the right show how a positive spin–spin coupling constant affects the energies. The transitions shown are for $\beta \leftarrow \alpha$ of A or X, the other nucleus (X or A, respectively) remaining unchanged. We have exaggerated the effect for clarity; in practice, the splitting caused by spin–spin coupling is much smaller than that caused by the applied field.

where ν_A and ν_X are the Larmor frequencies of A and X and m_A and m_X are their quantum numbers. This expression gives the four lines on the left of Fig. 15.11. The spin–spin coupling depends on the relative orientation of the two nuclear spins, so it is proportional to the product $m_A m_X$. Therefore, the energy including spin–spin coupling is

$$E = -h\nu_A m_A - h\nu_X m_X + hJm_A m_X \tag{15.25}$$

If $J > 0$, a lower energy is obtained when $m_A m_X < 0$, which is the case if one spin is α and the other is β. A higher energy is obtained if both spins are α or both spins are β. The opposite is true if $J < 0$. The resulting energy level diagram (for $J > 0$) is shown on the right of Fig. 15.11. We see that the $\alpha\alpha$ and $\beta\beta$ states are both raised by $\frac{1}{4}hJ$ and that the $\alpha\beta$ and $\beta\alpha$ states are both lowered by $\frac{1}{4}hJ$.

When a transition of nucleus A occurs, nucleus X remains unchanged. Therefore, the A resonance is a transition for which $\Delta m_A = +1$ and $\Delta m_X = 0$. There are two such transitions, one in which $\beta_A \leftarrow \alpha_A$ occurs when the X nucleus is α_X, and the other in which $\beta_A \leftarrow \alpha_A$ occurs when the X nucleus is β_X. They are shown in Fig. 15.11 and in a slightly different form in Fig. 15.12. The energies of the transitions are

$$\Delta E = h\nu_A \pm \tfrac{1}{2}hJ \tag{15.26a}$$

Therefore, the A resonance consists of a doublet of separation J centred on the chemical shift of A (Fig. 15.13). Similar remarks apply to the X resonance, which consists of two transitions according to whether the A nucleus is α or β (as shown in Fig. 15.12). The transition energies are

$$\Delta E = h\nu_X \pm \tfrac{1}{2}hJ \tag{15.26b}$$

It follows that the X resonance also consists of two lines of separation J, but they are centred on the chemical shift of X (as shown in Fig. 15.13).

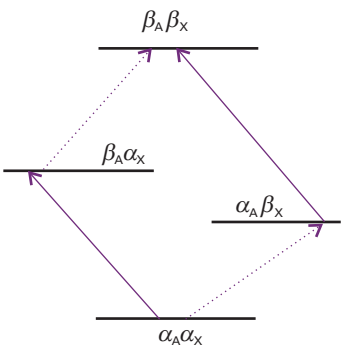

Fig. 15.12 An alternative depiction of the energy levels and transitions shown in Fig. 15.11. Once again, we have exaggerated the effect of spin–spin coupling.

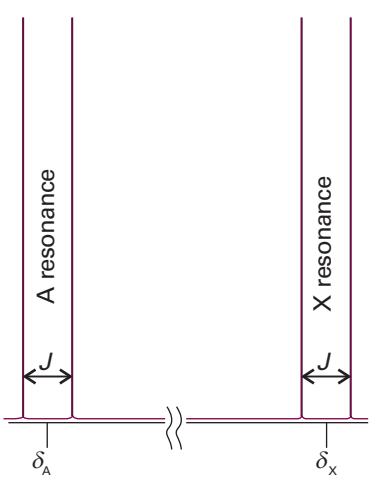

Fig. 15.13 The effect of spin–spin coupling on an AX spectrum. Each resonance is split into two lines separated by J. The pairs of resonances are centred on the chemical shifts of the protons in the absence of spin–spin coupling.

(b) Patterns of coupling

We have seen that in an AX system, spin–spin coupling will result in four lines in the NMR spectrum. Instead of a single line from A, we get a doublet of lines separated by J and centred on the chemical shift characteristic of A. The same splitting occurs in the X resonance: instead of a single line, the resonance is a doublet with splitting J (the same value as for the splitting of A) centred on the chemical shift characteristic of X. These features are summarized in Fig. 15.13.

A subtle point is that the X resonance in an AX_n species (such as an AX_2 or AX_3 species) is also a doublet with splitting J. As we shall explain below, *a group of equivalent nuclei resonates like a single nucleus*. The only difference for the X resonance of an AX_n species is that the intensity is n times as great as that of an AX species (Fig. 15.14). The A resonance in an AX_n species, though, is quite different from the A resonance in an AX species. For example, consider an AX_2 species with two equivalent X nuclei. The resonance of A is split into a doublet of separation J by one X, and each line of that doublet is split again by the same amount by the second X (Fig. 15.15). This splitting results in three lines in the intensity ratio 1:2:1 (because the central frequency can be obtained in two ways). The A resonance of an A_nX_2 species would also be a 1:2:1 triplet of splitting J, the only difference being that the intensity of the A resonance would be n times as great as that of AX_2.

Three equivalent X nuclei (an AX_3 species) split the resonance of A into four lines of intensity ratio 1:3:3:1 and separation J (Fig. 15.16). The X resonance, though, is still a doublet of separation J. In general, n equivalent spin-$\frac{1}{2}$ nuclei split the resonance of a nearby spin or group of equivalent spins into $n + 1$ lines with an intensity distribution given by 'Pascal's triangle' in which each entry is the sum of the two entries immediately above (**4**). The easiest way of constructing the pattern of fine structure is to draw a diagram in which successive rows show the splitting of a subsequent proton. The procedure is illustrated in Fig. 15.17 and was used in Figs. 15.15 and 15.16. It is easily extended to molecules containing nuclei with $I > \frac{1}{2}$ (Fig. 15.18).

			1			
		1		1		
	1		2		1	
1		3		3		1
	4		6		4	
1		5		10		10		5		1

4

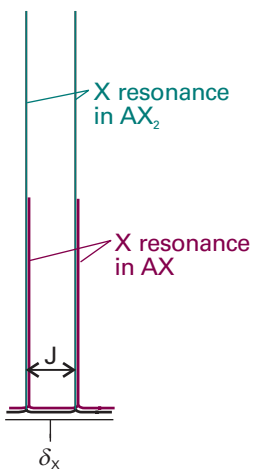

Fig. 15.14 The X resonance of an AX_2 species is also a doublet, because the two equivalent X nuclei behave like a single nucleus; however, the overall absorption is twice as intense as that of an AX species.

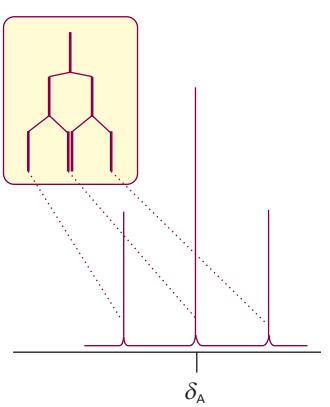

Fig. 15.15 The origin of the 1:2:1 triplet in the A resonance of an AX_2 species. The resonance of A is split into two by coupling with one X nucleus (as shown in the inset), and then each of those two lines is split into two by coupling to the second X nucleus. Because each X nucleus causes the same splitting, the two central transitions are coincident and give rise to an absorption line of double the intensity of the outer lines.

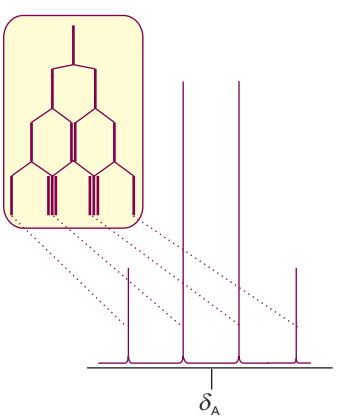

Fig. 15.16 The origin of the 1:3:3:1 quartet in the A resonance of an AX_3 species. The third X nucleus splits each of the lines shown in Fig. 15.15 for an AX_2 species into a doublet, and the intensity distribution reflects the number of transitions that have the same energy.

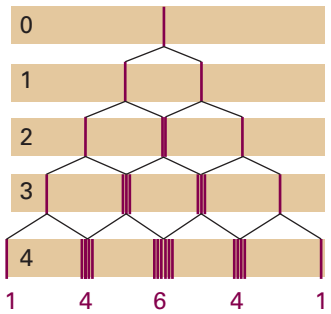

Fig. 15.17 The intensity distribution of the A resonance of an AX_n resonance can be constructed by considering the splitting caused by 1, 2, . . . *n* protons, as in Figs. 15.15 and 15.16. The resulting intensity distribution has a binomial distribution and is given by the integers in the corresponding row of Pascal's triangle. Note that, although the lines have been drawn side-by-side for clarity, the members of each group are coincident. Four protons, in AX_4, split the A resonance into a 1:4:6:4:1 quintet.

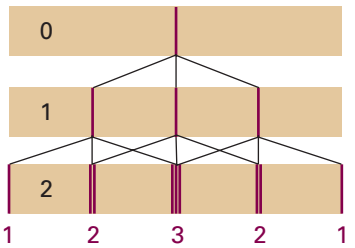

Fig. 15.18 The intensity distribution arising from spin–spin interaction with nuclei with $I = 1$ can be constructed similarly, but each successive nucleus splits the lines into three equal intensity components. Two equivalent spin-1 nuclei give rise to a 1:2:3:2:1 quintet.

Example 15.1 *Accounting for the fine structure in a spectrum*

Account for the fine structure in the NMR spectrum of the C—H protons of ethanol.

Method Consider how each group of equivalent protons (for instance, three methyl protons) split the resonances of the other groups of protons. There is no splitting within groups of equivalent protons. Each splitting pattern can be decided by referring to Pascal's triangle.

Answer The three protons of the CH_3 group split the resonance of the CH_2 protons into a 1:3:3:1 quartet with a splitting *J*. Likewise, the two protons of the CH_2 group split the resonance of the CH_3 protons into a 1:2:1 triplet with the same splitting *J*. The CH_2 and CH_3 protons all interact with the OH proton, but these couplings do not cause any splitting because the OH protons migrate rapidly from molecule to molecule and their effect averages to zero.

Self-test 15.2 What fine-structure can be expected for the protons in $^{14}NH_4^+$? The spin quantum number of nitrogen is 1. [1:1:1 triplet from N]

(c) The magnitudes of coupling constants

The scalar coupling constant of two nuclei separated by *N* bonds is denoted ^NJ, with subscripts for the types of nuclei involved. Thus, $^1J_{CH}$ is the coupling constant for a proton joined directly to a ^{13}C atom, and $^2J_{CH}$ is the coupling constant when the same two nuclei are separated by two bonds (as in $^{13}C—C—H$). A typical value of $^1J_{CH}$ is in the range 120 to 250 Hz; $^2J_{CH}$ is between −10 and +20 Hz. Both ^3J and ^4J can give detectable effects in a spectrum, but couplings over larger numbers of bonds can generally

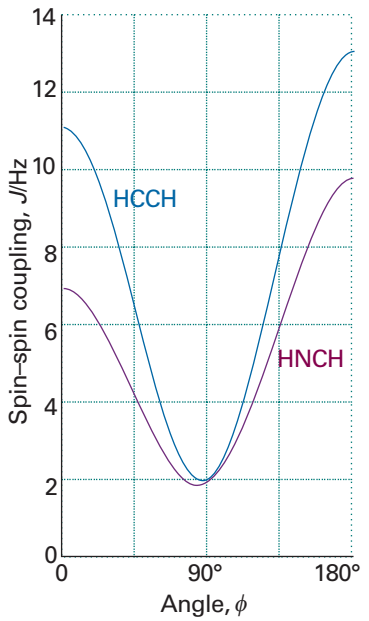

Fig. 15.19 The variation of the spin–spin coupling constant with angle predicted by the Karplus equation for an HCCH group and an HNCH group.

Exploration Draw a family of curves showing the variation of $^3J_{HH}$ with ϕ for which $A = +7.0$ Hz, $B = -1.0$ Hz, and C varies slightly from a typical value of +5.0 Hz. What is the effect of changing the value of the parameter C on the shape of the curve? In a similar fashion, explore the effect of the values of A and B on the shape of the curve.

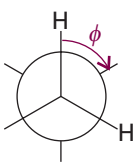

5

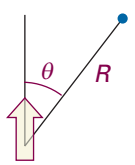

6

Comment 15.4

The average (or mean value) of a function $f(x)$ over the range $x = a$ to $x = b$ is $\int_a^b f(x)\mathrm{d}x/(b-a)$. The volume element in polar coordinates is proportional to $\sin\theta\,\mathrm{d}\theta$, and θ ranges from 0 to π. Therefore the average value of $(1 - 3\cos^2\theta)$ is $\int_0^\pi (1 - 3\cos^2\theta)\sin\theta\,\mathrm{d}\theta/\pi = 0$.

be ignored. One of the longest range couplings that has been detected is $^9J_{HH} = 0.4$ Hz between the CH_3 and CH_2 protons in $CH_3C{\equiv}CC{\equiv}CC{\equiv}CCH_2OH$.

The sign of J_{XY} indicates whether the energy of two spins is lower when they are parallel ($J < 0$) or when they are antiparallel ($J > 0$). It is found that $^1J_{CH}$ is often positive, $^2J_{HH}$ is often negative, $^3J_{HH}$ is often positive, and so on. An additional point is that J varies with the angle between the bonds (Fig. 15.19). Thus, a $^3J_{HH}$ coupling constant is often found to depend on the dihedral angle ϕ (**5**) according to the **Karplus equation**:

$$J = A + B\cos\phi + C\cos 2\phi \qquad (15.27)$$

with A, B, and C empirical constants with values close to +7 Hz, −1 Hz, and +5 Hz, respectively, for an HCCH fragment. It follows that the measurement of $^3J_{HH}$ in a series of related compounds can be used to determine their conformations. The coupling constant $^1J_{CH}$ also depends on the hybridization of the C atom, as the following values indicate:

	sp	sp^2	sp^3
$^1J_{CH}$/Hz:	250	160	125

(d) The origin of spin–spin coupling

Spin–spin coupling is a very subtle phenomenon, and it is better to treat J as an empirical parameter than to use calculated values. However, we can get some insight into its origins, if not its precise magnitude—or always reliably its sign—by considering the magnetic interactions within molecules.

A nucleus with spin projection m_I gives rise to a magnetic field with z-component $\mathcal{B}_{nuc}$ at a distance R, where, to a good approximation,

$$\mathcal{B}_{nuc} = -\frac{\gamma\hbar\mu_0}{4\pi R^3}(1 - 3\cos^2\theta)m_I \qquad (15.28)$$

The angle θ is defined in (**6**). The magnitude of this field is about 0.1 mT when $R = 0.3$ nm, corresponding to a splitting of resonance signal of about 10^4 Hz, and is of the order of magnitude of the splitting observed in solid samples (see Section 15.3a).

In a liquid, the angle θ sweeps over all values as the molecule tumbles, and $1–3\cos^2\theta$ averages to zero. Hence the direct dipolar interaction between spins cannot account for the fine structure of the spectra of rapidly tumbling molecules. The direct interaction does make an important contribution to the spectra of solid samples and is a very useful indirect source of structure information through its involvement in spin relaxation (Section 15.11).

Spin–spin coupling in molecules in solution can be explained in terms of the **polarization mechanism**, in which the interaction is transmitted through the bonds. The simplest case to consider is that of $^1J_{XY}$ where X and Y are spin-$\frac{1}{2}$ nuclei joined by an electron-pair bond (Fig. 15.20). The coupling mechanism depends on the fact that in some atoms it is favourable for the nucleus and a nearby electron spin to be parallel (both α or both β), but in others it is favourable for them to be antiparallel (one α and the other β). The electron–nucleus coupling is magnetic in origin, and may be either a dipolar interaction between the magnetic moments of the electron and nuclear spins or a **Fermi contact interaction**. A pictorial description of the Fermi contact interaction is as follows. First, we regard the magnetic moment of the nucleus as arising from the circulation of a current in a tiny loop with a radius similar to that of the nucleus (Fig. 15.21). Far from the nucleus the field generated by this loop is indistinguishable from the field generated by a point magnetic dipole. Close to the loop, however, the field differs from that of a point dipole. The magnetic interaction between this non-dipolar field and the electron's magnetic moment is the contact

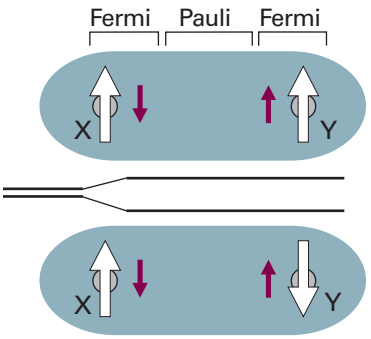

Fig. 15.20 The polarization mechanism for spin–spin coupling ($^1J_{HH}$). The two arrangements have slightly different energies. In this case, J is positive, corresponding to a lower energy when the nuclear spins are antiparallel.

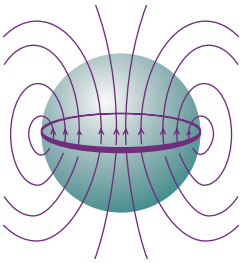

Fig. 15.21 The origin of the Fermi contact interaction. From far away, the magnetic field pattern arising from a ring of current (representing the rotating charge of the nucleus, the pale green sphere) is that of a point dipole. However, if an electron can sample the field close to the region indicated by the sphere, the field distribution differs significantly from that of a point dipole. For example, if the electron can penetrate the sphere, then the spherical average of the field it experiences is not zero.

interaction. The lines of force depicted in Fig. 15.21 correspond to those for a proton with α spin. The lower energy state of an electron spin in such a field is the β state. In conclusion, the contact interaction depends on the very close approach of an electron to the nucleus and hence can occur only if the electron occupies an *s* orbital (which is the reason why $^1J_{CH}$ depends on the hybridization ratio). We shall suppose that it is energetically favourable for an electron spin and a nuclear spin to be antiparallel (as is the case for a proton and an electron in a hydrogen atom).

If the X nucleus is α, a β electron of the bonding pair will tend to be found nearby (because that is energetically favourable for it). The second electron in the bond, which must have α spin if the other is β, will be found mainly at the far end of the bond (because electrons tend to stay apart to reduce their mutual repulsion). Because it is energetically favourable for the spin of Y to be antiparallel to an electron spin, a Y nucleus with β spin has a lower energy, and hence a lower Larmor frequency, than a Y nucleus with α spin. The opposite is true when X is β, for now the α spin of Y has the lower energy. In other words, the antiparallel arrangement of nuclear spins lies lower in energy than the parallel arrangement as a result of their magnetic coupling with the bond electrons. That is, $^1J_{HH}$ is positive.

To account for the value of $^2J_{XY}$, as in H—C—H, we need a mechanism that can transmit the spin alignments through the central C atom (which may be ^{12}C, with no nuclear spin of its own). In this case (Fig. 15.22), an X nucleus with α spin polarizes the electrons in its bond, and the α electron is likely to be found closer to the C nucleus. The more favourable arrangement of two electrons on the same atom is with their spins parallel (Hund's rule, Section 10.4d), so the more favourable arrangement is for the α electron of the neighbouring bond to be close to the C nucleus. Consequently, the β electron of that bond is more likely to be found close to the Y nucleus, and therefore that nucleus will have a lower energy if it is α. Hence, according to this mechanism, the lower Larmor frequency of Y will be obtained if its spin is parallel to that of X. That is, $^2J_{HH}$ is negative.

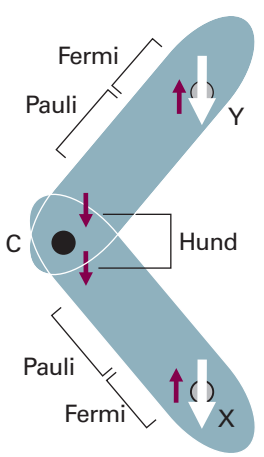

Fig. 15.22 The polarization mechanism for $^2J_{HH}$ spin–spin coupling. The spin information is transmitted from one bond to the next by a version of the mechanism that accounts for the lower energy of electrons with parallel spins in different atomic orbitals (Hund's rule of maximum multiplicity). In this case, $J < 0$, corresponding to a lower energy when the nuclear spins are parallel.

The coupling of nuclear spin to electron spin by the Fermi contact interaction is most important for proton spins, but it is not necessarily the most important mechanism for other nuclei. These nuclei may also interact by a dipolar mechanism with the electron magnetic moments and with their orbital motion, and there is no simple way of specifying whether J will be positive or negative.

(e) Equivalent nuclei

A group of nuclei are **chemically equivalent** if they are related by a symmetry operation of the molecule and have the same chemical shifts. Chemically equivalent nuclei are nuclei that would be regarded as 'equivalent' according to ordinary chemical criteria. Nuclei are **magnetically equivalent** if, as well as being chemically equivalent, they also have identical spin–spin interactions with any other magnetic nuclei in the molecule.

The difference between chemical and magnetic equivalence is illustrated by CH_2F_2 and $H_2C{=}CF_2$. In each of these molecules the protons are chemically equivalent: they are related by symmetry and undergo the same chemical reactions. However, although the protons in CH_2F_2 are magnetically equivalent, those in $CH_2{=}CF_2$ are not. One proton in the latter has a *cis* spin-coupling interaction with a given F nucleus whereas the other proton has a *trans* interaction with it. In constrast, in CH_2F_2 both protons are connected to a given F nucleus by identical bonds, so there is no distinction between them. Strictly speaking, the CH_3 protons in ethanol (and other compounds) are magnetically inequivalent on account of their different interactions with the CH_2 protons in the next group. However, they are in practice made magnetically equivalent by the rapid rotation of the CH_3 group, which averages out any differences. Magnetically inequivalent species can give very complicated spectra (for instance, the proton and ^{19}F spectra of $H_2C{=}CF_2$ each consist of 12 lines), and we shall not consider them further.

An important feature of chemically equivalent magnetic nuclei is that, although they do couple together, the coupling has no effect on the appearance of the spectrum. The reason for the invisibility of the coupling is set out in the following *Justification*, but qualitatively it is that all allowed nuclear spin transitions are *collective* reorientations of groups of equivalent nuclear spins that do not change the relative orientations of the spins within the group (Fig. 15.23). Then, because the relative orientations of nuclear spins are not changed in any transition, the magnitude of the coupling between them is undetectable. Hence, an isolated CH_3 group gives a single, unsplit line because all the allowed transitions of the group of three protons occur without change of their relative orientations.

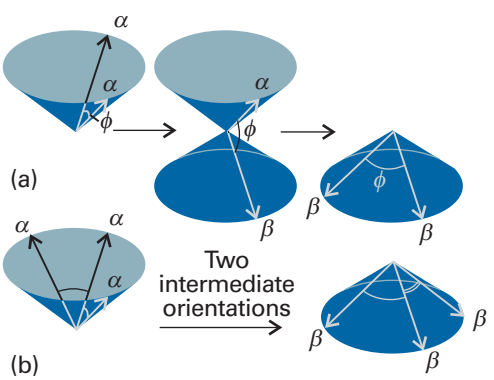

Fig. 15.23 (a) A group of two equivalent nuclei realigns as a group, without change of angle between the spins, when a resonant absorption occurs. Hence it behaves like a single nucleus and the spin–spin coupling between the individual spins of the group is undetectable. (b) Three equivalent nuclei also realign as a group without change of their relative orientations.

Justification 15.2 *The energy levels of an A_2 system*

Consider an A_2 system of two chemically equivalent spin-$\frac{1}{2}$ nuclei. First, consider the energy levels in the absence of spin–spin coupling. There are four spin states that (just as for two electrons) can be classified according to their total spin I (the analogue of S for two electrons) and their total projection M_I on the z-axis. The states are analogous to those we developed for two electrons in singlet and triplet states:

Spins parallel, $I = 1$:	$M_I = +1$	$\alpha\alpha$
	$M_I = 0$	$(1/2^{1/2})\{\alpha\beta + \beta\alpha\}$
	$M_I = -1$	$\beta\beta$
Spins paired, $I = 0$:	$M_I = 0$	$(1/2^{1/2})\{\alpha\beta - \beta\alpha\}$

The effect of a magnetic field on these four states is shown in Fig. 15.24: the energies of the two states with $M_I = 0$ are unchanged by the field because they are composed of equal proportions of α and β spins.

As remarked in Section 15.6a, the spin–spin coupling energy is proportional to the scalar product of the vectors representing the spins, $E = (hJ/\hbar^2)\boldsymbol{I}_1\cdot\boldsymbol{I}_2$. The scalar product can be expressed in terms of the total nuclear spin by noting that

$$I^2 = (\boldsymbol{I}_1 + \boldsymbol{I}_2)\cdot(\boldsymbol{I}_1 + \boldsymbol{I}_2) = I_1^2 + I_2^2 + 2\boldsymbol{I}_1\cdot\boldsymbol{I}_2$$

rearranging this expression to

$$\boldsymbol{I}_1\cdot\boldsymbol{I}_2 = \tfrac{1}{2}\{I^2 - I_1^2 - I_2^2\}$$

and replacing the magnitudes by their quantum mechanical values:

$$\boldsymbol{I}_1\cdot\boldsymbol{I}_2 = \tfrac{1}{2}\{I(I+1) - I_1(I_1+1) - I_2(I_2+1)\}\hbar^2$$

Then, because $I_1 = I_2 = \frac{1}{2}$, it follows that

$$E = \tfrac{1}{2}hJ\{I(I+1) - \tfrac{3}{2}\}$$

For parallel spins, $I = 1$ and $E = +\frac{1}{4}hJ$; for antiparallel spins $I = 0$ and $E = -\frac{3}{4}hJ$, as in Fig. 15.24. We see that three of the states move in energy in one direction and the fourth (the one with antiparallel spins) moves three times as much in the opposite direction. The resulting energy levels are shown on the right in Fig. 15.24.

Comment 15.5

As in Section 10.7, the states we have selected in *Justification* 15.2 are those with a definite resultant, and hence a well defined value of I. The + sign in $\alpha\beta + \beta\alpha$ signifies an in-phase alignment of spins and $I = 1$; the – sign in $\alpha\beta - \beta\alpha$ signifies an alignment out of phase by π, and hence $I = 0$. See Fig. 10.24.

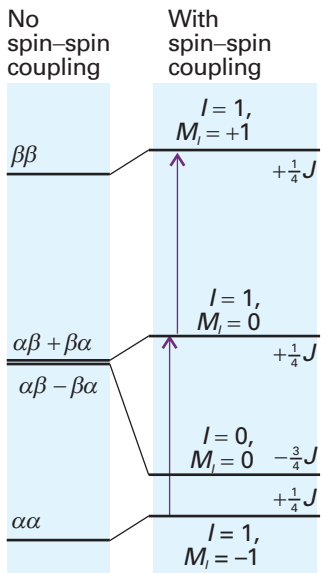

Fig. 15.24 The energy levels of an A_2 system in the absence of spin–spin coupling are shown on the left. When spin–spin coupling is taken into account, the energy levels on the right are obtained. Note that the three states with total nuclear spin $I = 1$ correspond to parallel spins and give rise to the same increase in energy (J is positive); the one state with $I = 0$ (antiparallel nuclear spins) has a lower energy in the presence of spin–spin coupling. The only allowed transitions are those that preserve the angle between the spins, and so take place between the three states with $I = 1$. They occur at the same resonance frequency as they would have in the absence of spin–spin coupling.

The NMR spectrum of the A_2 species arises from transitions between the levels. However, the radiofrequency field affects the two equivalent protons equally, so it cannot change the orientation of one proton relative to the other; therefore, the transitions take place within the set of states that correspond to parallel spin (those labelled $I = 1$), and no spin-parallel state can change to a spin-antiparallel state (the state with $I = 0$). Put another way, the allowed transitions are subject to the selection rule $\Delta I = 0$. This selection rule is in addition to the rule $\Delta M_I = \pm 1$ that arises from the conservation of angular momentum and the unit spin of the photon. The allowed transitions are shown in Fig. 15.24: we see that there are only two transitions, and that they occur at the same resonance frequency that the nuclei would have in the absence of spin–spin coupling. Hence, the spin–spin coupling interaction does not affect the appearance of the spectrum.

(f) Strongly coupled nuclei

NMR spectra are usually much more complex than the foregoing simple analysis suggests. We have described the extreme case in which the differences in chemical shifts

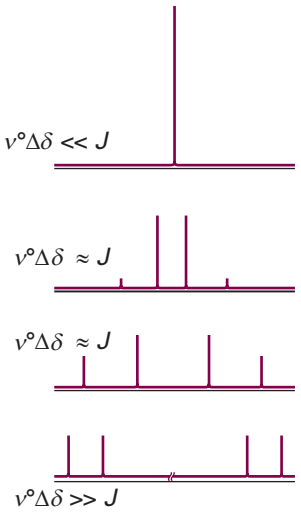

Fig. 15.25 The NMR spectra of an A_2 system (top) and an AX system (bottom) are simple 'first-order' spectra. At intermediate relative values of the chemical shift difference and the spin–spin coupling, complex 'strongly coupled' spectra are obtained. Note how the inner two lines of the bottom spectrum move together, grow in intensity, and form the single central line of the top spectrum. The two outer lines diminish in intensity and are absent in the top spectrum.

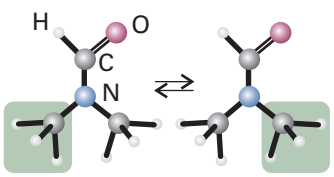

Fig. 15.26 When a molecule changes from one conformation to another, the positions of its protons are interchanged and jump between magnetically distinct environments.

are much greater than the spin–spin coupling constants. In such cases it is simple to identify groups of magnetically equivalent nuclei and to think of the groups of nuclear spins as reorientating relative to each other. The spectra that result are called **first-order spectra**.

Transitions cannot be allocated to definite groups when the differences in their chemical shifts are comparable to their spin–spin coupling interactions. The complicated spectra that are then obtained are called **strongly coupled spectra** (or 'second-order spectra') and are much more difficult to analyse (Fig. 15.25). Because the difference in resonance frequencies increases with field, but spin–spin coupling constants are independent of it, a second-order spectrum may become simpler (and first-order) at high fields because individual groups of nuclei become identifiable again.

A clue to the type of analysis that is appropriate is given by the notation for the types of spins involved. Thus, an AX spin system (which consists of two nuclei with a large chemical shift difference) has a first-order spectrum. An AB system, on the other hand (with two nuclei of similar chemical shifts), gives a spectrum typical of a strongly coupled system. An AX system may have widely different Larmor frequencies because A and X are nuclei of different elements (such as ^{13}C and ^{1}H), in which case they form a **heteronuclear spin system**. AX may also denote a **homonuclear spin system** in which the nuclei are of the same element but in markedly different environments.

15.7 Conformational conversion and exchange processes

The appearance of an NMR spectrum is changed if magnetic nuclei can jump rapidly between different environments. Consider a molecule, such as *N*,*N*-dimethylformamide, that can jump between conformations; in its case, the methyl shifts depend on whether they are *cis* or *trans* to the carbonyl group (Fig. 15.26). When the jumping rate is low, the spectrum shows two sets of lines, one each from molecules in each conformation. When the interconversion is fast, the spectrum shows a single line at the mean of the two chemical shifts. At intermediate inversion rates, the line is very broad. This maximum broadening occurs when the lifetime, τ, of a conformation gives rise to a linewidth that is comparable to the difference of resonance frequencies, $\delta\nu$, and both broadened lines blend together into a very broad line. Coalescence of the two lines occurs when

$$\tau = \frac{\sqrt{2}}{\pi\delta\nu} \qquad (15.29)$$

Example 15.2 *Interpreting line broadening*

The NO group in *N*,*N*-dimethylnitrosamine, $(CH_3)_2N{-}NO$, rotates about the N—N bond and, as a result, the magnetic environments of the two CH_3 groups are interchanged. The two CH_3 resonances are separated by 390 Hz in a 600 MHz spectrometer. At what rate of interconversion will the resonance collapse to a single line?

Method Use eqn 15.29 for the average lifetimes of the conformations. The rate of interconversion is the inverse of their lifetime.

Answer With $\delta\nu = 390$ Hz,

$$\tau = \frac{\sqrt{2}}{\pi \times (390\ \text{s}^{-1})} = 1.2\ \text{ms}$$

It follows that the signal will collapse to a single line when the interconversion rate exceeds about 830 s^{-1}. The dependence of the rate of exchange on the temperature is used to determine the energy barrier to interconversion.

Self-test 15.3 What would you deduce from the observation of a single line from the same molecule in a 300 MHz spectrometer?

[Conformation lifetime less than 2.3 ms]

A similar explanation accounts for the loss of fine structure in solvents able to exchange protons with the sample. For example, hydroxyl protons are able to exchange with water protons. When this **chemical exchange** occurs, a molecule ROH with an α-spin proton (we write this ROH_α) rapidly converts to ROH_β and then perhaps to ROH_α again because the protons provided by the solvent molecules in successive exchanges have random spin orientations. Therefore, instead of seeing a spectrum composed of contributions from both ROH_α and ROH_β molecules (that is, a spectrum showing a doublet structure due to the OH proton) we see a spectrum that shows no splitting caused by coupling of the OH proton (as in Fig. 15.6). The effect is observed when the lifetime of a molecule due to this chemical exchange is so short that the lifetime broadening is greater than the doublet splitting. Because this splitting is often very small (a few hertz), a proton must remain attached to the same molecule for longer than about 0.1 s for the splitting to be observable. In water, the exchange rate is much faster than that, so alcohols show no splitting from the OH protons. In dry dimethylsulfoxide (DMSO), the exchange rate may be slow enough for the splitting to be detected.

Pulse techniques in NMR

Modern methods of detecting the energy separation between nuclear spin states are more sophisticated than simply looking for the frequency at which resonance occurs. One of the best analogies that has been suggested to illustrate the difference between the old and new ways of observing an NMR spectrum is that of detecting the spectrum of vibrations of a bell. We could stimulate the bell with a gentle vibration at a gradually increasing frequency, and note the frequencies at which it resonated with the stimulation. A lot of time would be spent getting zero response when the stimulating frequency was between the bell's vibrational modes. However, if we were simply to hit the bell with a hammer, we would immediately obtain a clang composed of all the frequencies that the bell can produce. The equivalent in NMR is to monitor the radiation nuclear spins emit as they return to equilibrium after the appropriate stimulation. The resulting **Fourier-transform NMR** gives greatly increased sensitivity, so opening up the entire periodic table to the technique. Moreover, multiple-pulse FT-NMR gives chemists unparalleled control over the information content and display of spectra. We need to understand how the equivalent of the hammer blow is delivered and how the signal is monitored and interpreted. These features are generally expressed in terms of the vector model of angular momentum introduced in Section 9.7d.

15.8 The magnetization vector

Consider a sample composed of many identical spin-$\frac{1}{2}$ nuclei. As we saw in Section 9.7d, an angular momentum can be represented by a vector of length $\{I(I+1)\}^{1/2}$ units

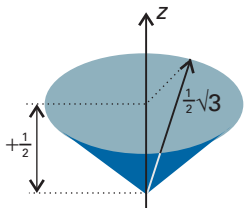

Fig. 15.27 The vector model of angular momentum for a single spin-$\frac{1}{2}$ nucleus. The angle around the z-axis is indeterminate.

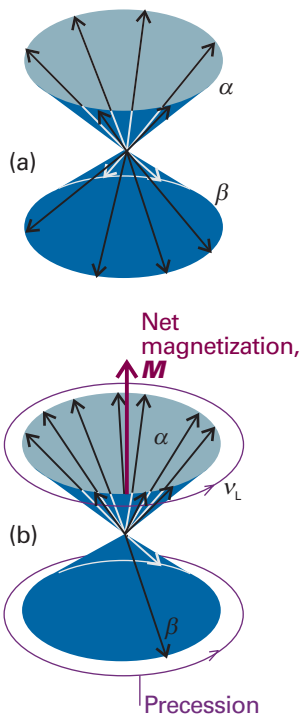

Fig. 15.28 The magnetization of a sample of spin-$\frac{1}{2}$ nuclei is the resultant of all their magnetic moments. (a) In the absence of an externally applied field, there are equal numbers of α and β spins at random angles around the z-axis (the field direction) and the magnetization is zero. (b) In the presence of a field, the spins precess around their cones (that is, there is an energy difference between the α and β states) and there are slightly more α spins than β spins. As a result, there is a net magnetization along the z-axis.

with a component of length m_I units along the z-axis. As the uncertainty principle does not allow us to specify the x- and y-components of the angular momentum, all we know is that the vector lies somewhere on a cone around the z-axis. For $I = \frac{1}{2}$, the length of the vector is $\frac{1}{2}\sqrt{3}$ and it makes an angle of 55° to the z-axis (Fig. 15.27).

In the absence of a magnetic field, the sample consists of equal numbers of α and β nuclear spins with their vectors lying at random angles on the cones. These angles are unpredictable, and at this stage we picture the spin vectors as stationary. The **magnetization**, $\boldsymbol{M}$, of the sample, its net nuclear magnetic moment, is zero (Fig. 15.28a).

(a) The effect of the static field

Two changes occur in the magnetization when a magnetic field is present. First, the energies of the two orientations change, the α spins moving to low energy and the β spins to high energy (provided $\gamma > 0$). At 10 T, the Larmor frequency for protons is 427 MHz, and in the vector model the individual vectors are pictured as precessing at this rate. This motion is a pictorial representation of the difference in energy of the spin states (it is not an actual representation of reality). As the field is increased, the Larmor frequency increases and the precession becomes faster. Secondly, the populations of the two spin states (the numbers of α and β spins) at thermal equilibrium change, and there will be more α spins than β spins. Because $h\nu_L/kT \approx 7 \times 10^{-5}$ for protons at 300 K and 10 T, it follows from the Boltzmann distribution that $N_\beta/N_\alpha = e^{-h\nu_L/kT}$ is only slightly less than 1. That is, there is only a tiny imbalance of populations, and it is even smaller for other nuclei with their smaller magnetogyric ratios. However, despite its smallness, the imbalance means that there is a net magnetization that we can represent by a vector $\boldsymbol{M}$ pointing in the z-direction and with a length proportional to the population difference (Fig. 15.28b).

(b) The effect of the radiofrequency field

We now consider the effect of a radiofrequency field circularly polarized in the xy-plane, so that the magnetic component of the electromagnetic field (the only component we need to consider) is rotating around the z-direction, the direction of the applied field $\mathcal{B}_0$, in the same sense as the Larmor precession. The strength of the rotating magnetic field is $\mathcal{B}_1$. Suppose we choose the frequency of this field to be equal to the Larmor frequency of the spins, $\nu_L = (\gamma/2\pi)\mathcal{B}_0$; this choice is equivalent to selecting the resonance condition in the conventional experiment. The nuclei now experience a steady $\mathcal{B}_1$ field because the rotating magnetic field is in step with the precessing spins (Fig. 15.29a). Just as the spins precess about the strong static field $\mathcal{B}_0$ at a frequency $\gamma\mathcal{B}_0/2\pi$, so under the influence of the field $\mathcal{B}_1$ they precess about $\mathcal{B}_1$ at a frequency $\gamma\mathcal{B}_1/2\pi$.

To interpret the effects of radiofrequency pulses on the magnetization, it is often useful to look at the spin system from a different perspective. If we were to imagine stepping on to a platform, a so-called **rotating frame**, that rotates around the direction of the applied field at the radiofrequency, then the nuclear magnetization appears stationary if the radiofrequency is the same as the Larmor frequency (Fig. 15.29b). If the $\mathcal{B}_1$ field is applied in a pulse of duration $\pi/2\gamma\mathcal{B}_1$, the magnetization tips through 90° in the rotating frame and we say that we have applied a **90° pulse**, or a '$\pi/2$ pulse' (Fig. 15.30a). The duration of the pulse depends on the strength of the $\mathcal{B}_1$ field, but is typically of the order of microseconds.

Now imagine stepping out of the rotating frame. To an external observer (the role played by a radiofrequency coil) in this stationary frame, the magnetization vector is now rotating at the Larmor frequency in the xy-plane (Fig. 15.30b). The rotating magnetization induces in the coil a signal that oscillates at the Larmor frequency and that

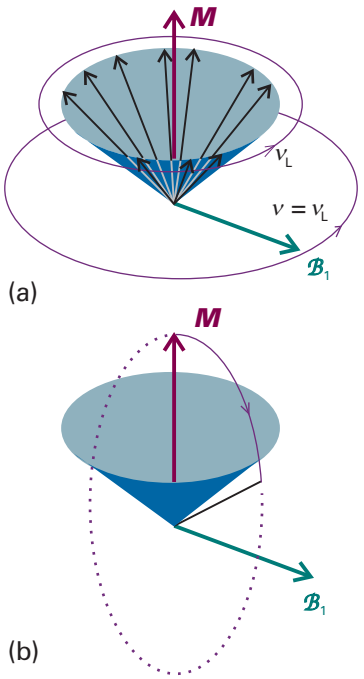

Fig. 15.29 (a) In a resonance experiment, a circularly polarized radiofrequency magnetic field $\mathcal{B}_1$ is applied in the *xy*-plane (the magnetization vector lies along the *z*-axis). (b) If we step into a frame rotating at the radiofrequency, $\mathcal{B}_1$ appears to be stationary, as does the magnetization ***M*** if the Larmor frequency is equal to the radiofrequency. When the two frequencies coincide, the magnetization vector of the sample rotates around the direction of the $\mathcal{B}_1$ field.

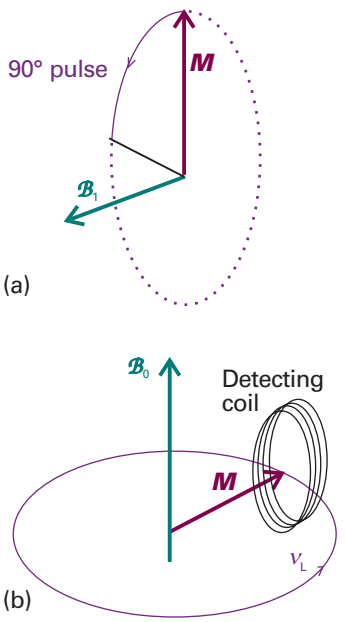

Fig. 15.30 (a) If the radiofrequency field is applied for a certain time, the magnetization vector is rotated into the *xy*-plane. (b) To an external stationary observer (the coil), the magnetization vector is rotating at the Larmor frequency, and can induce a signal in the coil.

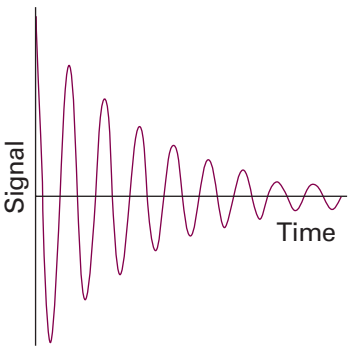

Fig. 15.31 A simple free-induction decay of a sample of spins with a single resonance frequency.

can be amplified and processed. In practice, the processing takes place after subtraction of a constant high frequency component (the radiofrequency used for $\mathcal{B}_1$), so that all the signal manipulation takes place at frequencies of a few kilohertz.

As time passes, the individual spins move out of step (partly because they are precessing at slightly different rates, as we shall explain later), so the magnetization vector shrinks exponentially with a time constant T_2 and induces an ever weaker signal in the detector coil. The form of the signal that we can expect is therefore the oscillating-decaying **free-induction decay** (FID) shown in Fig. 15.31. The *y*-component of the magnetization varies as

$$M_y(t) = M_0 \cos(2\pi\nu_L t)\, e^{-t/T_2} \qquad (15.30)$$

We have considered the effect of a pulse applied at exactly the Larmor frequency. However, virtually the same effect is obtained off resonance, provided that the pulse is applied close to ν_L. If the difference in frequency is small compared to the inverse of the duration of the 90° pulse, the magnetization will end up in the *xy*-plane. Note that we do not need to know the Larmor frequency beforehand: the short pulse is the analogue of the hammer blow on the bell, exciting a range of frequencies. The detected signal shows that a particular resonant frequency is present.

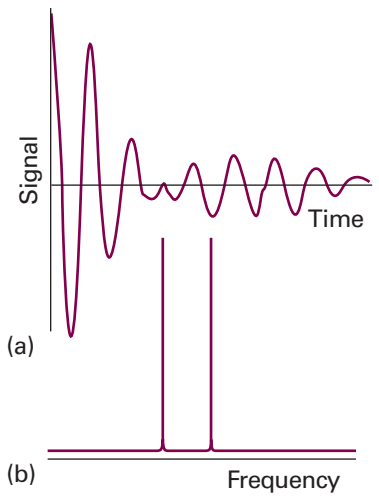

Fig. 15.32 (a) A free induction decay signal of a sample of AX species and (b) its analysis into its frequency components.

Exploration The *Living graphs* section of the text's web site has an applet that allows you to calculate and display the FID curve from an AX system. Explore the effect on the shape of the FID curve of changing the chemical shifts (and therefore the Larmor frequencies) of the A and X nuclei.

Comment 15.6

The web site for this text contains links to databases of NMR spectra and to sites that allow for interactive simulation of NMR spectra.

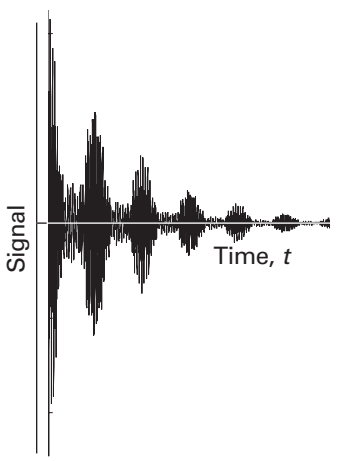

Fig. 15.33 A free induction decay signal of a sample of ethanol. Its Fourier transform is the frequency-domain spectrum shown in Fig. 15.6. The total length of the image corresponds to about 1 s.

(c) Time- and frequency-domain signals

We can think of the magnetization vector of a homonuclear AX spin system with $J = 0$ as consisting of two parts, one formed by the A spins and the other by the X spins. When the 90° pulse is applied, both magnetization vectors are rotated into the xy-plane. However, because the A and X nuclei precess at different frequencies, they induce two signals in the detector coils, and the overall FID curve may resemble that in Fig. 15.32a. The composite FID curve is the analogue of the struck bell emitting a rich tone composed of all the frequencies at which it can vibrate.

The problem we must address is how to recover the resonance frequencies present in a free-induction decay. We know that the FID curve is a sum of oscillating functions, so the problem is to analyse it into its component frequencies by carrying out a Fourier transformation (*Further information* 13.2 and 15.1). When the signal in Fig.15.32a is transformed in this way, we get the frequency-domain spectrum shown in Fig. 15.32b. One line represents the Larmor frequency of the A nuclei and the other that of the X nuclei.

The FID curve in Fig. 15.33 is obtained from a sample of ethanol. The frequency-domain spectrum obtained from it by Fourier transformation is the one that we have already discussed (Fig. 15.6). We can now see why the FID curve in Fig. 15.33 is so complex: it arises from the precession of a magnetization vector that is composed of eight components, each with a characteristic frequency.

15.9 Spin relaxation

There are two reasons why the component of the magnetization vector in the xy-plane shrinks. Both reflect the fact that the nuclear spins are not in thermal equilibrium with their surroundings (for then $\boldsymbol{M}$ lies parallel to z). The return to equilibrium is the process called **spin relaxation**.

(a) Longitudinal and transverse relaxation

At thermal equilibrium the spins have a Boltzmann distribution, with more α spins than β spins; however, a magnetization vector in the xy-plane immediately after a 90° pulse has equal numbers of α and β spins.

Now consider the effect of a **180° pulse**, which may be visualized in the rotating frame as a flip of the net magnetization vector from one direction along the z-axis to the opposite direction. That is, the 180° pulse leads to population inversion of the spin system, which now has more β spins than α spins. After the pulse, the populations revert to their thermal equilibrium values exponentially. As they do so, the z-component of magnetization reverts to its equilibrium value M_0 with a time constant called the **longitudinal relaxation time**, T_1 (Fig. 15.34):

$$M_z(t) - M_0 \propto \mathrm{e}^{-t/T_1} \tag{15.31}$$

Because this relaxation process involves giving up energy to the surroundings (the 'lattice') as β spins revert to α spins, the time constant T_1 is also called the **spin–lattice relaxation time**. Spin–lattice relaxation is caused by local magnetic fields that fluctuate at a frequency close to the resonance frequency of the $\alpha \rightarrow \beta$ transition. Such fields can arise from the tumbling motion of molecules in a fluid sample. If molecular tumbling is too slow or too fast compared to the resonance frequency, it will give rise to a fluctuating magnetic field with a frequency that is either too low or too high to stimulate a spin change from β to α, so T_1 will be long. Only if the molecule tumbles at about the resonance frequency will the fluctuating magnetic field be able to induce spin changes effectively, and only then will T_1 be short. The rate of molecular tumbling

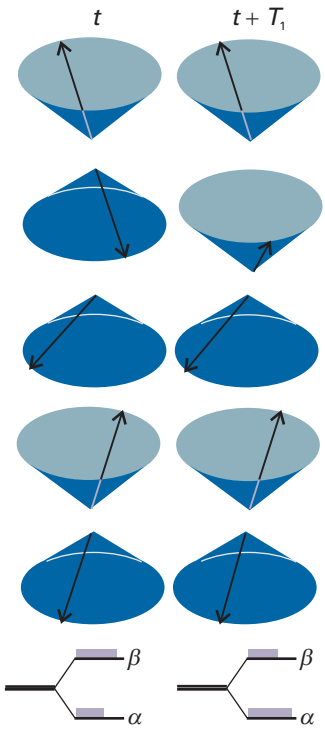

Fig. 15.34 In longitudinal relaxation the spins relax back towards their thermal equilibrium populations. On the left we see the precessional cones representing spin-$\frac{1}{2}$ angular momenta, and they do not have their thermal equilibrium populations (there are more α-spins than β-spins). On the right, which represents the sample a long time after a time T_1 has elapsed, the populations are those characteristic of a Boltzmann distribution (see *Molecular interpretation 3.1*). In actuality, T_1 is the time constant for relaxation to the arrangement on the right and T_1 ln 2 is the half-life of the arrangement on the left.

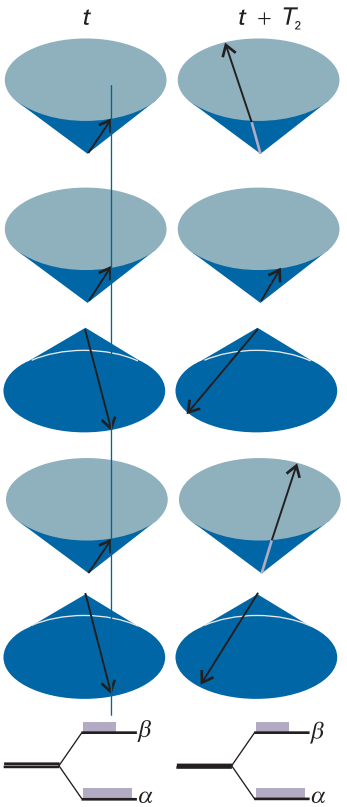

Fig. 15.36 The transverse relaxation time, T_2, is the time constant for the phases of the spins to become randomized (another condition for equilibrium) and to change from the orderly arrangement shown on the left to the disorderly arrangement on the right (long after a time T_2 has elapsed). Note that the populations of the states remain the same; only the relative phase of the spins relaxes. In actuality, T_2 is the time constant for relaxation to the arrangement on the right and T_2 ln 2 is the half-life of the arrangement on the left.

increases with temperature and with reducing viscosity of the solvent, so we can expect a dependence like that shown in Fig. 15.35.

A second aspect of spin relaxation is the fanning-out of the spins in the *xy*-plane if they precess at different rates (Fig. 15.36). The magnetization vector is large when all the spins are bunched together immediately after a 90° pulse. However, this orderly bunching of spins is not at equilibrium and, even if there were no spin–lattice relaxation, we would expect the individual spins to spread out until they were uniformly distributed with all possible angles around the *z*-axis. At that stage, the component of magnetization vector in the plane would be zero. The randomization of the spin directions occurs exponentially with a time constant called the **transverse relaxation time**, T_2:

$$M_y(t) \propto e^{-t/T_2} \qquad (15.32)$$

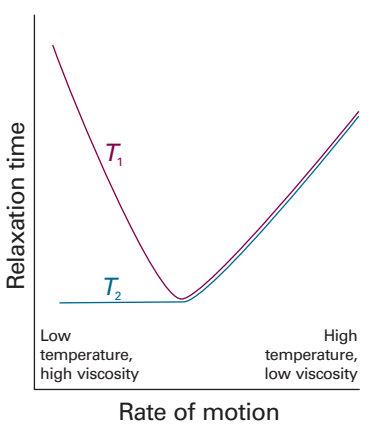

Fig. 15.35 The variation of the two relaxation times with the rate at which the molecules move (either by tumbling or migrating through the solution). The horizontal axis can be interpreted as representing temperature or viscosity. Note that, at rapid rates of motion, the two relaxation times coincide.

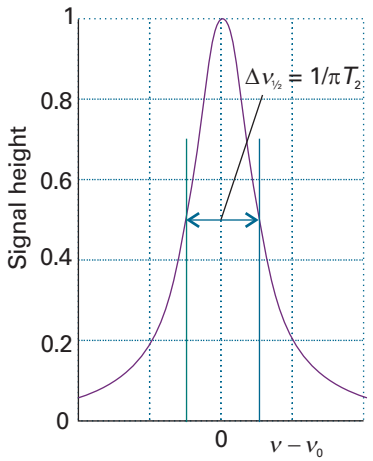

Fig. 15.37 A Lorentzian absorption line. The width at half-height is inversely proportional to the parameter T_2 and the longer the transverse relaxation time, the narrower the line.

Exploration The *Living graphs* section of the text's web site has an applet that allows you to calculate and display Lorenztian absorption lines. Explore the effect of the parameter T_2 on the width and the maximal intensity of a Lorentzian line. Rationalize your observations.

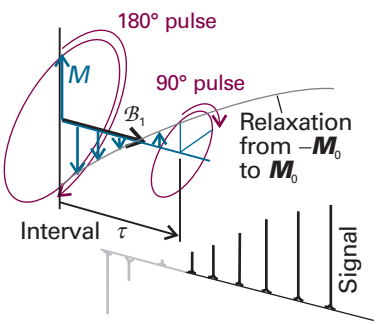

Fig. 15.38 The result of applying a 180° pulse to the magnetization in the rotating frame and the effect of a subsequent 90° pulse. The amplitude of the frequency-domain spectrum varies with the interval between the two pulses because spin–lattice relaxation has time to occur.

Because the relaxation involves the relative orientation of the spins, T_2 is also known as the **spin–spin relaxation time**. Any relaxation process that changes the balance between α and β spins will also contribute to this randomization, so the time constant T_2 is almost always less than or equal to T_1.

Local magnetic fields also affect spin–spin relaxation. When the fluctuations are slow, each molecule lingers in its local magnetic environment and the spin orientations randomize quickly around the applied field direction. If the molecules move rapidly from one magnetic environment to another, the effects of differences in local magnetic field average to zero: individual spins do not precess at very different rates, they can remain bunched for longer, and spin–spin relaxation does not take place as quickly. In other words, slow molecular motion corresponds to short T_2 and fast motion corresponds to long T_2 (as shown in Fig. 15.35). Calculations show that, when the motion is fast, $T_2 \approx T_1$.

If the y-component of magnetization decays with a time constant T_2, the spectral line is broadened (Fig. 15.37), and its width at half-height becomes

$$\Delta\nu_{1/2} = \frac{1}{\pi T_2} \tag{15.33}$$

Typical values of T_2 in proton NMR are of the order of seconds, so linewidths of around 0.1 Hz can be anticipated, in broad agreement with observation.

So far, we have assumed that the equipment, and in particular the magnet, is perfect, and that the differences in Larmor frequencies arise solely from interactions within the sample. In practice, the magnet is not perfect, and the field is different at different locations in the sample. The inhomogeneity broadens the resonance, and in most cases this **inhomogeneous broadening** dominates the broadening we have discussed so far. It is common to express the extent of inhomogeneous broadening in terms of an **effective transverse relaxation time**, T_2^*, by using a relation like eqn 15.33, but writing

$$T_2^* = \frac{1}{\pi\Delta\nu_{1/2}} \tag{15.34}$$

where $\Delta\nu_{1/2}$ is the observed width at half-height of a line with a Lorenztian shape of the form $I \propto 1/(1+\nu^2)$. As an example, consider a line in a spectrum with a width of 10 Hz. It follows from eqn 15.34 that the effective transverse relaxation time is

$$T_2^* = \frac{1}{\pi \times (10\ \mathrm{s}^{-1})} = 32\ \mathrm{ms}$$

(b) The measurement of T_1

The longitudinal relaxation time T_1 can be measured by the **inversion recovery technique**. The first step is to apply a 180° pulse to the sample. A 180° pulse is achieved by applying the $\mathcal{B}_1$ field for twice as long as for a 90° pulse, so the magnetization vector precesses through 180° and points in the $-z$-direction (Fig. 15.38). No signal can be seen at this stage because there is no component of magnetization in the xy-plane (where the coil can detect it). The β spins begin to relax back into α spins, and the magnetization vector first shrinks exponentially, falling through zero to its thermal equilibrium value, M_z. After an interval τ, a 90° pulse is applied that rotates the magnetization into the xy-plane, where it generates an FID signal. The frequency-domain spectrum is then obtained by Fourier transformation.

The intensity of the spectrum obtained in this way depends on the length of the magnetization vector that is rotated into the *xy*-plane. The length of that vector changes exponentially as the interval between the two pulses is increased, so the intensity of the spectrum also changes exponentially with increasing τ. We can therefore measure T_1 by fitting an exponential curve to the series of spectra obtained with different values of τ.

(c) Spin echoes

The measurement of T_2 (as distinct from T_2^*) depends on being able to eliminate the effects of inhomogeneous broadening. The cunning required is at the root of some of the most important advances that have been made in NMR since its introduction.

A **spin echo** is the magnetic analogue of an audible echo: transverse magnetization is created by a radiofrequency pulse, decays away, is reflected by a second pulse, and grows back to form an echo. The sequence of events is shown in Fig. 15.39. We can consider the overall magnetization as being made up of a number of different magnetizations, each of which arises from a **spin packet** of nuclei with very similar precession frequencies. The spread in these frequencies arises because the applied field $\mathcal{B}_0$ is inhomogeneous, so different parts of the sample experience different fields. The precession frequencies also differ if there is more than one chemical shift present. As will be seen, the importance of a spin echo is that it can suppress the effects of both field inhomogeneities and chemical shifts.

First, a 90° pulse is applied to the sample. We follow events by using the rotating frame, in which $\mathcal{B}_1$ is stationary along the *x*-axis and causes the magnetization to be into the *xy*-plane. The spin packets now begin to fan out because they have different Larmor frequencies, with some above the radiofrequency and some below. The detected signal depends on the resultant of the spin-packet magnetization vectors, and decays with a time-constant T_2^* because of the combined effects of field inhomogeneity and spin–spin relaxation.

After an evolution period τ, a 180° pulse is applied to the sample; this time, about the *y*-axis of the rotating frame (the axis of the pulse is changed from *x* to *y* by a 90° phase shift of the radiofrequency radiation). The pulse rotates the magnetization vectors of the faster spin packets into the positions previously occupied by the slower spin packets, and vice versa. Thus, as the vectors continue to precess, the fast vectors are now behind the slow; the fan begins to close up again, and the resultant signal begins to grow back into an echo. At time 2τ, all the vectors will once more be aligned along the *y*-axis, and the fanning out caused by the field inhomogeneity is said to have been **refocused**: the spin echo has reached its maximum. Because the effects of field inhomogeneities have been suppressed by the refocusing, the echo signal will have been attenuated by the factor $e^{-2\tau/T_2}$ caused by spin–spin relaxation alone. After the time 2τ, the magnetization will continue to precess, fanning out once again, giving a resultant that decays with time constant T_2^*.

The important feature of the technique is that the size of the echo is independent of any local fields that remain constant during the two τ intervals. If a spin packet is 'fast' because it happens to be composed of spins in a region of the sample that experiences higher than average fields, then it remains fast throughout both intervals, and what it gains on the first interval it loses on the second interval. Hence, the size of the echo is independent of inhomogeneities in the magnetic field, for these remain constant. The true transverse relaxation arises from fields that vary on a molecular distance scale, and there is no guarantee that an individual 'fast' spin will remain 'fast' in the refocusing phase: the spins within the packets therefore spread with a time constant T_2. Hence, the effects of the true relaxation are not refocused, and the size of the echo decays with the time constant T_2 (Fig. 15.40).

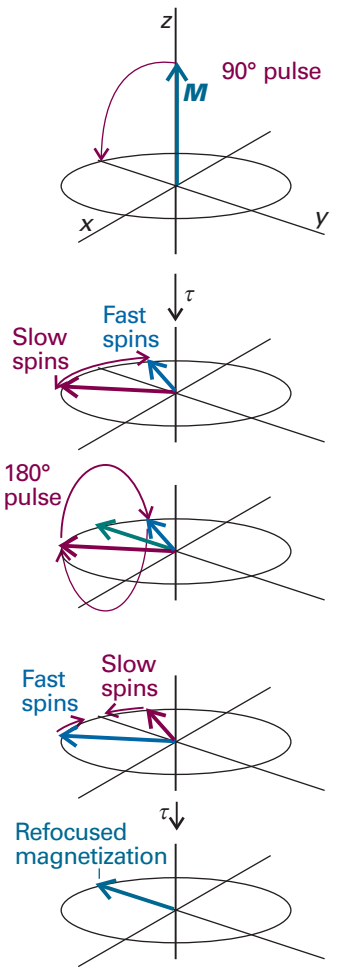

Fig. 15.39 The sequence of pulses leading to the observation of a spin echo.

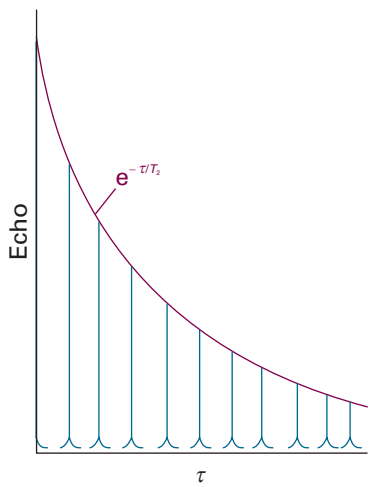

Fig. 15.40 The exponential decay of spin echoes can be used to determine the transverse relaxation time.

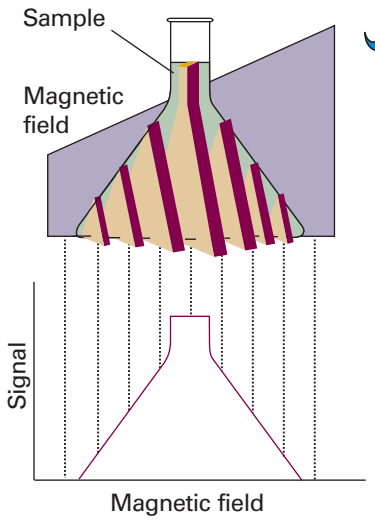

Fig. 15.41 In a magnetic field that varies linearly over a sample, all the protons within a given slice (that is, at a given field value) come into resonance and give a signal of the corresponding intensity. The resulting intensity pattern is a map of the numbers in all the slices, and portrays the shape of the sample. Changing the orientation of the field shows the shape along the corresponding direction, and computer manipulation can be used to build up the three-dimensional shape of the sample.

IMPACT ON MEDICINE

I15.1 Magnetic resonance imaging

One of the most striking applications of nuclear magnetic resonance is in medicine. *Magnetic resonance imaging* (MRI) is a portrayal of the concentrations of protons in a solid object. The technique relies on the application of specific pulse sequences to an object in an inhomogeneous magnetic field.

If an object containing hydrogen nuclei (a tube of water or a human body) is placed in an NMR spectrometer and exposed to a *homogeneous* magnetic field, then a single resonance signal will be detected. Now consider a flask of water in a magnetic field that varies linearly in the z-direction according to $\mathcal{B}_0 + G_z z$, where G_z is the field gradient along the z-direction (Fig. 15.41). Then the water protons will be resonant at the frequencies

$$\nu_{\mathrm{L}}(z) = \frac{\gamma}{2\pi}(\mathcal{B}_0 + G_z z) \tag{15.35}$$

(Similar equations may be written for gradients along the x- and y-directions.) Application of a 90° radiofrequency pulse with $\nu = \nu_{\mathrm{L}}(z)$ will result in a signal with an intensity that is proportional to the numbers of protons at the position z. This is an example of *slice selection*, the application of a selective 90° pulse that excites nuclei in a specific region, or slice, of the sample. It follows that the intensity of the NMR signal will be a projection of the numbers of protons on a line parallel to the field gradient. The image of a three-dimensional object such as a flask of water can be obtained if the slice selection technique is applied at different orientations (see Fig. 15.41). In *projection reconstruction*, the projections can be analysed on a computer to reconstruct the three-dimensional distribution of protons in the object.

In practice, the NMR signal is not obtained by direct analysis of the FID curve after application of a single 90° pulse. Instead, spin echoes are often detected with several variations of the 90°–τ–180° pulse sequence (Section 15.9c). In *phase encoding*, field gradients are applied during the evolution period and the detection period of a spin-echo pulse sequence. The first step consists of a 90° pulse that results in slice selection along the z-direction. The second step consists of application of a *phase gradient*, a field gradient along the y-direction, during the evolution period. At each position along the gradient, a spin packet will precess at a different Larmor frequency due to chemical shift effects and the field inhomogeneity, so each packet will dephase to a different extent by the end of the evolution period. We can control the extent of dephasing by changing the duration of the evolution period, so Fourier transformation on τ gives information about the location of a proton along the y-direction.[1] For each value of τ, the next steps are application of the 180° pulse and then of a *read gradient*, a field gradient along the x-direction, during detection of the echo. Protons at different positions along x experience different fields and will resonate at different frequencies. Therefore Fourier transformation of the FID gives different signals for protons at different positions along x.

A common problem with the techniques described above is image contrast, which must be optimized in order to show spatial variations in water content in the sample. One strategy for solving this problem takes advantage of the fact that the relaxation times of water protons are shorter for water in biological tissues than for the pure liquid. Furthermore, relaxation times from water protons are also different in healthy and diseased tissues. A T_1-*weighted image* is obtained by repeating the spin echo sequence

[1] For technical reasons, it is more common to vary the magnitude of the phase gradient. See *Further reading* for details.

before spin–lattice relaxation can return the spins in the sample to equilibrium. Under these conditions, differences in signal intensities are directly related to differences in T_1. A *T_2-weighted image* is obtained by using an evolution period τ that is relatively long. Each point on the image is an echo signal that behaves in the manner shown in Fig. 15.40, so signal intensities are strongly dependent on variations in T_2. However, allowing so much of the decay to occur leads to weak signals even for those protons with long spin–spin relaxation times. Another strategy involves the use of *contrast agents*, paramagnetic compounds that shorten the relaxation times of nearby protons. The technique is particularly useful in enhancing image contrast and in diagnosing disease if the contrast agent is distributed differently in healthy and diseased tissues.

The MRI technique is used widely to detect physiological abnormalities and to observe metabolic processes. With *functional MRI*, blood flow in different regions of the brain can be studied and related to the mental activities of the subject. The technique is based on differences in the magnetic properties of deoxygenated and oxygenated haemoglobin, the iron-containing protein that transports O_2 in red blood cells. The more paramagnetic deoxygenated haemoglobin affects the proton resonances of tissue differently from the oxygenated protein. Because there is greater blood flow in active regions of the brain than in inactive regions, changes in the intensities of proton resonances due to changes in levels of oxygenated haemoglobin can be related to brain activity.

The special advantage of MRI is that it can image *soft* tissues (Fig. 15.42), whereas X-rays are largely used for imaging hard, bony structures and abnormally dense regions, such as tumours. In fact, the invisibility of hard structures in MRI is an advantage, as it allows the imaging of structures encased by bone, such as the brain and the spinal cord. X-rays are known to be dangerous on account of the ionization they cause; the high magnetic fields used in MRI may also be dangerous but, apart from anecdotes about the extraction of loose fillings from teeth, there is no convincing evidence of their harmfulness, and the technique is considered safe.

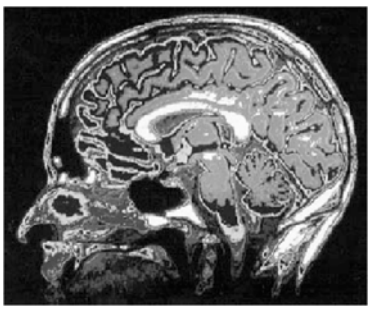

Fig. 15.42 The great advantage of MRI is that it can display soft tissue, such as in this cross-section through a patient's head. (Courtesy of the University of Manitoba.)

15.10 Spin decoupling

Carbon-13 is a **dilute-spin species** in the sense that it is unlikely that more than one ^{13}C nucleus will be found in any given small molecule (provided the sample has not been enriched with that isotope; the natural abundance of ^{13}C is only 1.1 per cent). Even in large molecules, although more than one ^{13}C nucleus may be present, it is unlikely that they will be close enough to give an observable splitting. Hence, it is not normally necessary to take into account $^{13}C—^{13}C$ spin–spin coupling within a molecule.

Protons are **abundant-spin species** in the sense that a molecule is likely to contain many of them. If we were observing a ^{13}C-NMR spectrum, we would obtain a very complex spectrum on account of the coupling of the one ^{13}C nucleus with many of the protons that are present. To avoid this difficulty, ^{13}C-NMR spectra are normally observed using the technique of **proton decoupling**. Thus, if the CH_3 protons of ethanol are irradiated with a second, strong, resonant radiofrequency pulse, they undergo rapid spin reorientations and the ^{13}C nucleus senses an average orientation. As a result, its resonance is a single line and not a 1:3:3:1 quartet. Proton decoupling has the additional advantage of enhancing sensitivity, because the intensity is concentrated into a single transition frequency instead of being spread over several transition frequencies (see Section 15.11). If care is taken to ensure that the other parameters on which the strength of the signal depends are kept constant, the intensities of proton-decoupled spectra are proportional to the number of ^{13}C nuclei present. The technique is widely used to characterize synthetic polymers.

Comment 15.7

In a dipole–dipole interaction between two nuclei, one nucleus influences the behaviour of another nucleus in much the same way that the orientation of a bar magnet is influenced by the presence of another bar magnet nearby. Dipole–dipole interactions are discussed in Chapter 18.

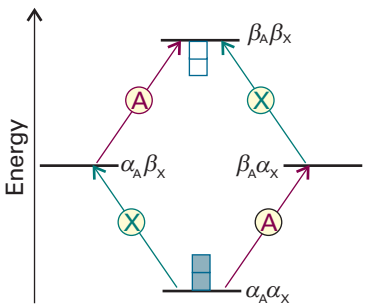

Fig. 15.43 The energy levels of an AX system and an indication of their relative populations. Each grey square above the line represents an excess population and each white square below the line represents a population deficit. The transitions of A and X are marked.

15.11 The nuclear Overhauser effect

We have seen already that one advantage of protons in NMR is their high magnetogyric ratio, which results in relatively large Boltzmann population differences and hence greater resonance intensities than for most other nuclei. In the steady-state **nuclear Overhauser effect** (NOE), spin relaxation processes involving internuclear dipole–dipole interactions are used to transfer this population advantage to another nucleus (such as ^{13}C or another proton), so that the latter's resonances are modified.

To understand the effect, we consider the populations of the four levels of a homonuclear (for instance, proton) AX system; these were shown in Fig. 15.12. At thermal equilibrium, the population of the $\alpha_A\alpha_X$ level is the greatest, and that of the $\beta_A\beta_X$ level is the least; the other two levels have the same energy and an intermediate population. The thermal equilibrium absorption intensities reflect these populations as shown in Fig. 15.43. Now consider the combined effect of spin relaxation and keeping the X spins saturated. When we saturate the X transition, the populations of the X levels are equalized ($N_{\alpha X} = N_{\beta X}$) and all transitions involving $\alpha_X \leftrightarrow \beta_X$ spin flips are no longer observed. At this stage there is no change in the populations of the A levels. If that were all there were to happen, all we would see would be the loss of the X resonance and no effect on the A resonance.

Now consider the effect of spin relaxation. Relaxation can occur in a variety of ways if there is a dipolar interaction between the A and X spins. One possibility is for the magnetic field acting between the two spins to cause them both to flop from β to α, so the $\alpha_A\alpha_X$ and $\beta_A\beta_X$ states regain their thermal equilibrium populations. However, the populations of the $\alpha_A\beta_X$ and $\beta_A\alpha_X$ levels remain unchanged at the values characteristic of saturation. As we see from Fig. 15.44, the population difference between the states joined by transitions of A is now greater than at equilibrium, so the resonance absorption is enhanced. Another possibility is for the dipolar interaction between the two spins to cause α to flip to β and β to flop to α. This transition equilibrates the populations of $\alpha_A\beta_X$ and $\beta_A\alpha_X$ but leaves the $\alpha_A\alpha_X$ and $\beta_A\beta_X$ populations unchanged. Now we see from the illustration that the population differences in the states involved in the A transitions are decreased, so the resonance absorption is diminished.

Which effect wins? Does the NOE enhance the A absorption or does it diminish it? As in the discussion of relaxation times in Section 15.9, the efficiency of the intensity-enhancing $\beta_A\beta_X \leftrightarrow \alpha_A\alpha_X$ relaxation is high if the dipole field oscillates at a frequency close to the transition frequency, which in this case is about 2ν; likewise, the efficiency

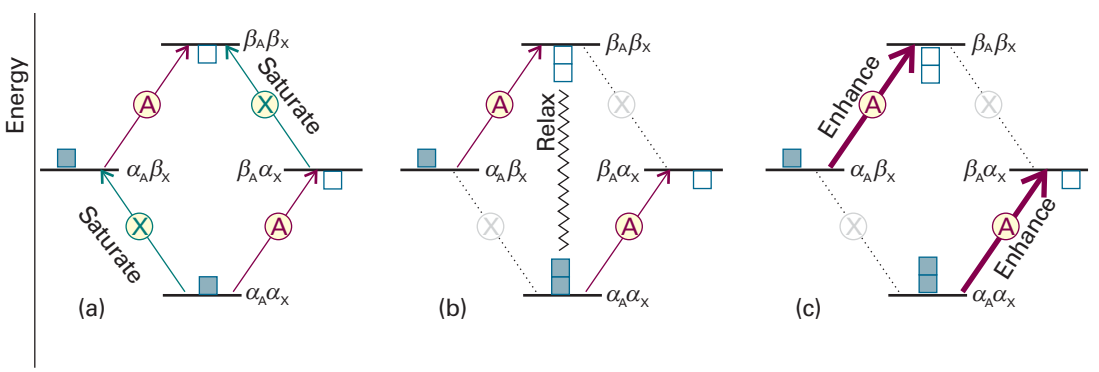

Fig. 15.44 (a) When the X transition is saturated, the populations of its two states are equalized and the population excess and deficit become as shown (using the same symbols as in Fig. 15.43). (b) Dipole–dipole relaxation relaxes the populations of the highest and lowest states, and they regain their original populations. (c) The A transitions reflect the difference in populations resulting from the preceding changes, and are enhanced compared with those shown in Fig. 15.43.

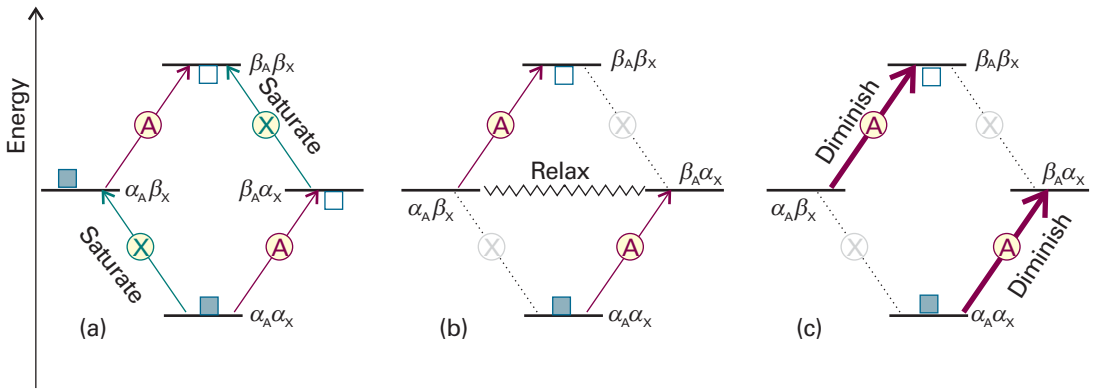

Fig. 15.45 (a) When the X transition is saturated, just as in Fig. 15.44 the populations of its two states are equalized and the population excess and deficit become as shown. (b) Dipole–dipole relaxation relaxes the populations of the two intermediate states, and they regain their original populations. (c) The A transitions reflect the difference in populations resulting from the preceding changes, and are diminished compared with those shown in Fig. 15.41.

of the intensity-diminishing $\alpha_A\beta_X \leftrightarrow \beta_A\alpha_X$ relaxation is high if the dipole field is stationary (as there is no frequency difference between the initial and final states). A large molecule rotates so slowly that there is very little motion at 2ν, so we expect an intensity decrease (Fig. 15.45). A small molecule rotating rapidly can be expected to have substantial motion at 2ν, and a consequent enhancement of the signal. In practice, the enhancement lies somewhere between the two extremes and is reported in terms of the parameter η (eta), where

$$\eta = \frac{I_A - I_A^\circ}{I_A^\circ} \qquad [15.36]$$

Here I_A° and I_A are the intensities of the NMR signals due to nucleus A before and after application of the long ($> T_1$) radiofrequency pulse that saturates transitions due to the X nucleus. When A and X are nuclei of the same species, such as protons, η lies between -1 (diminution) and $+\frac{1}{2}$ (enhancement). However, η also depends on the values of the magnetogyric ratios of A and X. In the case of maximal enhancement it is possible to show that

$$\eta = \frac{\gamma_X}{2\gamma_A} \qquad (15.37)$$

where γ_A and γ_X are the magnetogyric ratios of nuclei A and X, respectively. For ^{13}C close to a saturated proton, the ratio evaluates to 1.99, which shows that an enhancement of about a factor of 2 can be achieved.

The NOE is also used to determine interproton distances. The Overhauser enhancement of a proton A generated by saturating a spin X depends on the fraction of A's spin–lattice relaxation that is caused by its dipolar interaction with X. Because the dipolar field is proportional to r^{-3}, where r is the internuclear distance, and the relaxation effect is proportional to the square of the field, and therefore to r^{-6}, the NOE may be used to determine the geometries of molecules in solution. The determination of the structure of a small protein in solution involves the use of several hundred NOE measurements, effectively casting a net over the protons present. The enormous importance of this procedure is that we can determine the conformation of biological macromolecules in an aqueous environment and do not need to try to make the single crystals that are essential for an X-ray diffraction investigation (Chapter 20).

15.12 Two-dimensional NMR

An NMR spectrum contains a great deal of information and, if many protons are present, is very complex. Even a first-order spectrum is complex, for the fine structure of different groups of lines can overlap. The complexity would be reduced if we could use two axes to display the data, with resonances belonging to different groups lying at different locations on the second axis. This separation is essentially what is achieved in **two-dimensional NMR**.

All two-dimensional NMR experiments use the **PEMD pulse structure**, which consists of:

P: a *preparation period*, in which the spins first return to thermal equilibrium and then are excited by one or more radiofrequency pulses

E: an *evolution period* of duration t_1, during which the spins precess under the influence of their chemical shifts and spin–spin couplings

M: a *mixing period*, in which pulses may be used to transfer information between spins

D: a *detection period* of duration t_2, during which the FID is recorded.

Now we shall see how the PEMD pulse structure can be used to devise experiments that reveal spin–spin couplings and internuclear distances in small and large molecules.

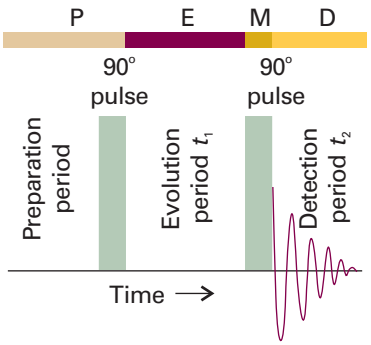

Fig. 15.46 The pulse sequence used in correlation spectroscopy (COSY). The preparation period is much longer than either T_1 or T_2, so the spins have time to relax before the next cycle of pulses begins. Acquisitions of free-induction decays are taken during t_2 for a set of different evolution times t_1. Fourier transformation on both variables t_1 and t_2 results in a two-dimensional spectrum, such as that shown in Fig 15.52.

(a) Correlation spectroscopy

Much modern NMR work makes use of techniques such as **correlation spectroscopy** (COSY) in which a clever choice of pulses and Fourier transformation techniques makes it possible to determine all spin–spin couplings in a molecule. The basic COSY experiment uses the simplest of all two-dimensional pulse sequences, consisting of two consecutive 90° pulses (Fig. 15.46).

To see how we can obtain a two-dimensional spectrum from a COSY experiment, we consider a trivial but illustrative example: the spectrum of a compound containing one proton, such as trichloromethane (chloroform, $CHCl_3$). Figure 15.47 shows the effect of the pulse sequence on the magnetization of the sample, which is aligned initially along the z-axis with a magnitude M_0. A 90° pulse applied in the x-direction (in the stationary frame) tilts the magnetization vector toward the y-axis. Then, during the evolution period, the magnetization vector rotates in the xy-plane with a frequency ν. At a time t_1 the vector will have swept through an angle $2\pi\nu t_1$ and the magnitude of the magnetization will have decayed by spin–spin relaxation to $M = M_0 e^{-t_1/T_2}$. By trigonometry, the magnitudes of the components of the magnetization vector are:

$$M_x = M \sin 2\pi\nu t_1 \qquad M_y = M \cos 2\pi\nu t_1 \qquad M_z = 0 \tag{15.38a}$$

Application of the second 90° pulse parallel to the x-axis tilts the magnetization again and the resulting vector has components with magnitudes (once again, in the stationary frame)

$$M_x = M \sin 2\pi\nu t_1 \qquad M_y = 0 \qquad M_z = M \cos 2\pi\nu t_1 \tag{15.38b}$$

The FID is detected over a period t_2 and Fourier transformation yields a signal over a frequency range ν_2 with a peak at ν, the resonance frequency of the proton. The signal intensity is related to M_x, the magnitude of the magnetization that is rotating around the xy-plane at the time of application of the detection pulse, so it follows that the signal strength varies sinusoidally with the duration of the evolution period. That is, if we were to acquire a series of spectra at different evolution times t_1, then we would obtain data as shown in Fig. 15.48a.

Comment 15.8

A vector, v, of length v, in the xy-plane and its two components, v_x and v_y, can be thought of as forming a right-angled triangle, with v the length of the hypotenuse (see the illustration). If θ is the angle that v_y makes with v, then it follows that $v_x = v \sin\theta$ and $v_y = v \cos\theta$.

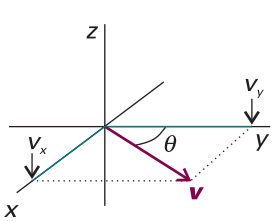

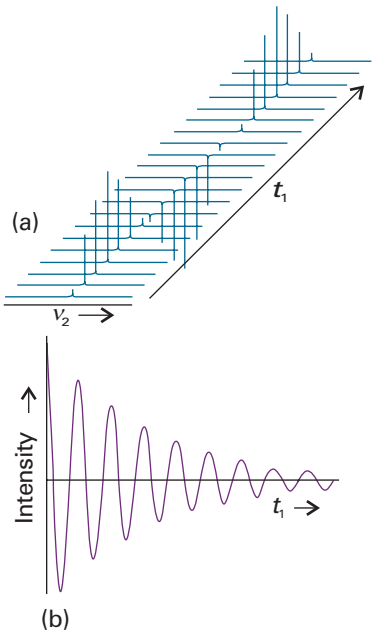

Fig. 15.48 (a) Spectra acquired for different evolution times t_1 between two 90° pulses. (b) A plot of the maximum intensity of each absorption line against t_1. Fourier transformation of this plot leads to a spectrum centred at ν, the resonance frequency of the protons in the sample.

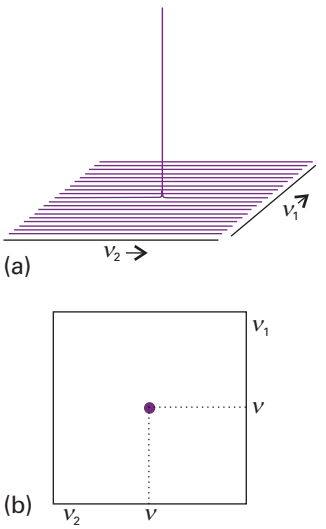

Fig. 15.49 (a) The two-dimensional NMR spectrum of the sample discussed in Figs. 15.47 and 15.48. See the text for an explanation of how the spectrum is obtained from a series of Fourier transformations of the data. (b) The contour plot of the spectrum in (a).

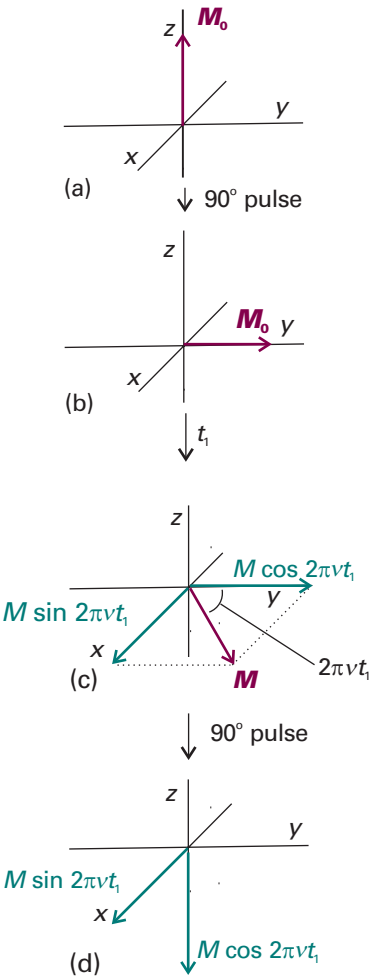

Fig. 15.47 (a) The effect of the pulse sequence shown in Fig. 15.46 on the magnetization $\boldsymbol{M}_0$ of a sample of a compound with only one proton. (b) A 90° pulse applied in the x-direction tilts the magnetization vector toward the y-axis. (c) After a time t_1 has elapsed, the vector will have swept through an angle $2\pi\nu t_1$ and the magnitude of the magnetization will have decayed to $\boldsymbol{M}$. The magnitudes of the components of $\boldsymbol{M}$ are $M_x = M \sin 2\pi\nu t_1$, $M_y = M \cos 2\pi\nu t_1$, and $M_z = 0$. (d) Application of the second 90° pulse parallel to the x-axis tilts the magnetization again and the resulting vector has components with magnitude $M_x = M \sin 2\pi\nu t_1$, $M_y = 0$, and $M_z = M \cos 2\pi\nu t_1$. The FID is detected at this stage of the experiment.

A plot of the maximum intensity of each absorption band in Fig. 15.48a against t_1 has the form shown in Fig. 15.48b. The plot resembles an FID curve with the oscillating component having a frequency ν, so Fourier transformation yields a signal over a frequency range ν_1 with a peak at ν. If we continue the process by first plotting signal intensity against t_1 for several frequencies along the ν_2 axis and then carrying out Fourier transformations, we generate a family of curves that can be pooled together into a three-dimensional plot of $I(\nu_1,\nu_2)$, the signal intensity as a function of the frequencies ν_1 and ν_2 (Fig. 15.49a). This plot is referred to as a *two-dimensional NMR spectrum* because Fourier transformations were performed in two variables. The most common representation of the data is as a contour plot, such as the one shown in Fig. 15.49b.

The experiment described above is not necessary for as simple a system as chloroform because the information contained in the two-dimensional spectrum could have been obtained much more quickly through the conventional, one-dimensional approach. However, when the one-dimensional spectrum is complex, the COSY experiment shows which spins are related by spin–spin coupling. To justify this statement, we now examine a spin-coupled AX system.

From our discussion so far, we know that the key to the COSY technique is the effect of the second 90° pulse. In this more complex example we consider its role for the four energy levels of an AX system (as shown in Fig. 15.12). At thermal equilibrium, the population of the $\alpha_A\alpha_X$ level is the greatest, and that of the $\beta_A\beta_X$ level is the least; the other two levels have the same energy and an intermediate population. After the first 90° pulse, the spins are no longer at thermal equilibrium. If a second 90° pulse

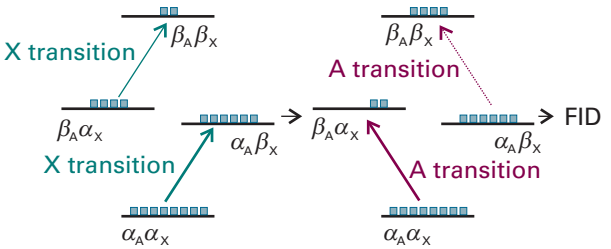

Fig. 15.50 An example of the change in the population of energy levels of an AX spin system that results from the second 90° pulse of a COSY experiment. Each square represents the same large number of spins. In this example, we imagine that the pulse affects the X spins first, and then the A spins. Excitation of the X spins inverts the populations of the $\beta_A\beta_X$ and $\beta_A\alpha_X$ levels and does not affect the populations of the $\alpha_A\alpha_X$ and $\alpha_A\beta_X$ levels. As a result, excitation of the A spins by the pulse generates an FID in which one of the two A transitions has increased in intensity and the other has decreased. That is, magnetization has been transferred from the X spins to the A spins. Similar schemes can be written to show that magnetization can be transferred from the A spins to the X spins.

is applied at a time t_1 that is short compared to the spin–lattice relaxation time T_1, the extra input of energy causes further changes in the populations of the four states. The changes in populations of the four states of the AX system will depend on how far the individual magnetizations have precessed during the evolution period. It is difficult to visualize these changes because the A spins are affecting the X spins and vice-versa.

For simplicity, we imagine that the second pulse induces X and A transitions sequentially. Depending on the evolution time t_1, the 90° pulse may leave the population differences across each of the two X transitions unchanged, inverted, or somewhere in between. Consider the extreme case in which one population difference is inverted and the other unchanged (Fig. 15.50). Excitation of the A transitions will now generate an FID in which one of the two A transitions has increased in intensity (because the population difference is now greater), and the other has decreased (because the population difference is now smaller). The overall effect is that precession of the X spins during the evolution period determines the amplitudes of the signals from the A spins obtained during the detection period. As the evolution time t_1 is increased, the intensities of the signals from A spins oscillate with frequencies determined by the frequencies of the two X transitions. Of course, it is just as easy to turn our scenario around and to conclude that the intensities of signals from X spins oscillate with frequencies determined by the frequencies of the A transitions.

This transfer of information between spins is at the heart of two-dimensional NMR spectroscopy: it leads to the *correlation* between different signals in a spectrum. In this case, information transfer tells us that there is spin–spin coupling between A and X. So, just as before, if we conduct a series of experiments in which t_1 is incremented, Fourier transformation of the FIDs on t_2 yields a set of spectra $I(t_1,F_2)$ in which the signal amplitudes oscillate as a function of t_1. A second Fourier transformation, now on t_1, converts these oscillations into a two-dimensional spectrum $I(F_1,F_2)$. The signals are spread out in F_1 according to their precession frequencies during the detection period. Thus, if we apply the COSY pulse sequence (Fig. 15.46) to the AX spin system, the result is a two-dimensional spectrum that contains four groups of signals in F_1 and F_2 centred on the two chemical shifts (Fig. 15.51). Each group consists of a block of four signals separated by J. The **diagonal peaks** are signals centred on (δ_A,δ_A) and (δ_X,δ_X) and lie along the diagonal $F_1 = F_2$. That is, the spectrum along the diagonal is equivalent to the one-dimensional spectrum obtained with the conventional NMR technique (Fig. 15.13). The **cross-peaks** (or *off-diagonal peaks*) are signals centred on (δ_A,δ_X) and (δ_X,δ_A) and owe their existence to the coupling between A and X.

Although information from two-dimensional NMR spectroscopy is trivial in an AX system, it can be of enormous help in the interpretation of more complex spectra, leading to a map of the couplings between spins and to the determination of the bonding network in complex molecules. Indeed, the spectrum of a synthetic or biological polymer that would be impossible to interpret in one-dimensional NMR but can often be interpreted reasonably rapidly by two-dimensional NMR. Below we illustrate the procedure by assigning the resonances in the COSY spectrum of an amino acid.

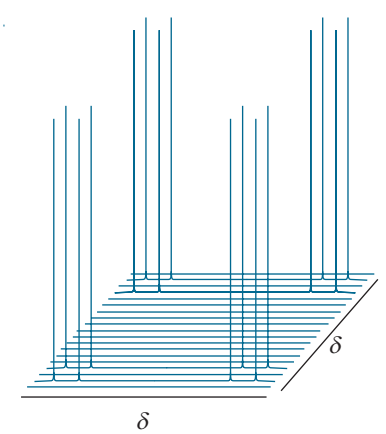

Fig. 15.51 A representation of the two-dimensional NMR spectrum obtained by application of the COSY pulse sequence to an AX spin system.

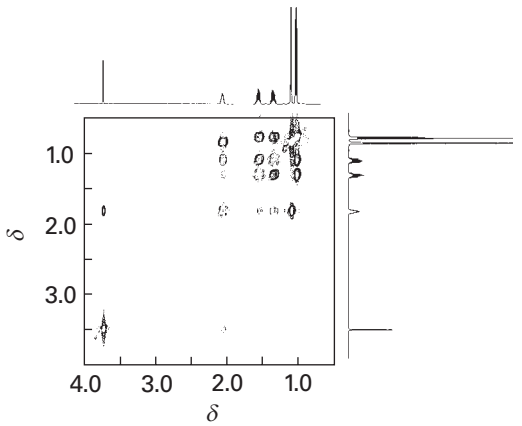

Fig. 15.52 Proton COSY spectrum of isoleucine. (Adapted from K.E. van Holde, W.C. Johnson, and P.S. Ho, *Principles of physical biochemistry*, p. 508, Prentice Hall, Upper Saddle River (1998).)

Illustration 15.3 *The COSY spectrum of isoleucine*

Figure 15.52 is a portion of the COSY spectrum of the amino acid isoleucine (**7**), showing the resonances associated with the protons bound to the carbon atoms. We begin the assignment process by considering which protons should be interacting by spin–spin coupling. From the known molecular structure, we conclude that:

1. The C_a—H proton is coupled only to the C_b—H proton.
2. The C_b—H protons are coupled to the C_a—H, C_c—H, and C_d—H protons.
3. The inequivalent C_d—H protons are coupled to the C_b—H and C_e—H protons.

We now note that:

- The resonance with $\delta = 3.6$ shares a cross-peak with only one other resonance at $\delta = 1.9$, which in turn shares cross-peaks with resonances at $\delta = 1.4$, 1.2, and 0.9. This identification is consistent with the resonances at $\delta = 3.6$ and 1.9 corresponding to the C_a—H and C_b—H protons, respectively.
- The proton with resonance at $\delta = 0.8$ is not coupled to the C_b—H protons, so we assign the resonance at $\delta = 0.8$ to the C_e—H protons.
- The resonances at $\delta = 1.4$ and 1.2 do not share cross-peaks with the resonance at $\delta = 0.9$.

In the light of the expected couplings, we assign the resonance at $\delta = 0.9$ to the C_c—H protons and the resonances at $\delta = 1.4$ and 1.2 to the inequivalent C_d—H protons.

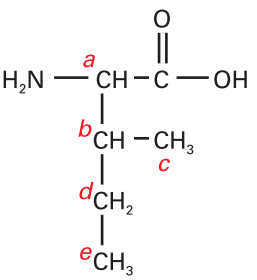

7 Isoleucine

Our simplified description of the COSY experiment does not reveal some important details. For example, the second 90° pulse actually mixes the spin state transitions caused by the first 90° pulse (hence the term 'mixing period'). Each of the four transitions (two for A and two for X) generated by the first pulse can be converted into any of the other three, or into formally forbidden **multiple quantum transitions**, which have $|\Delta m| > 1$. The latter transitions cannot generate any signal in the receiver coil of the spectrometer, but their existence can be demonstrated by applying a third pulse to mix them back into the four observable single quantum transitions. Many modern NMR experiments exploit multiple quantum transitions to filter out unwanted signals and to simplify spectra for interpretation.

(b) Nuclear Overhauser effect spectroscopy

Many different two-dimensional NMR experiments are based on the PEMD pulse structure. We have seen that the steady-state nuclear Overhauser effect can provide information about internuclear distances through analysis of enhancement patterns in the NMR spectrum before and after saturation of selected resonances. In its dynamic analogue, **nuclear Overhauser effect spectroscopy** (NOESY), the second 90° pulse of the COSY experiment is replaced by two 90° pulses separated by a time delay during which dipole–dipole interactions cause magnetization to be exchanged between neighbouring spins (Fig. 15.50). The results of double Fourier transformation is a spectrum in which the cross-peaks form a map of all the NOE interactions in a molecule. Because the nuclear Overhauser effect depends on the inverse sixth power of the separation between nuclei (see Section 15.11), NOESY data reveal internuclear distances up to about 0.5 nm.

15.13 Solid-state NMR

The principal difficulty with the application of NMR to solids is the low resolution characteristic of solid samples. Nevertheless, there are good reasons for seeking to overcome these difficulties. They include the possibility that a compound of interest is unstable in solution or that it is insoluble, so conventional solution NMR cannot be employed. Moreover, many species are intrinsically interesting as solids, and it is important to determine their structures and dynamics. Synthetic polymers are particularly interesting in this regard, and information can be obtained about the arrangement of molecules, their conformations, and the motion of different parts of the chain. This kind of information is crucial to an interpretation of the bulk properties of the polymer in terms of its molecular characteristics. Similarly, inorganic substances, such as the zeolites that are used as molecular sieves and shape-selective catalysts, can be studied using solid-state NMR, and structural problems can be resolved that cannot be tackled by X-ray diffraction.

Problems of resolution and linewidth are not the only features that plague NMR studies of solids, but the rewards are so great that considerable efforts have been made to overcome them and have achieved notable success. Because molecular rotation has almost ceased (except in special cases, including 'plastic crystals' in which the molecules continue to tumble), spin–lattice relaxation times are very long but spin–spin relaxation times are very short. Hence, in a pulse experiment, there is a need for lengthy delays—of several seconds—between successive pulses so that the spin system has time to revert to equilibrium. Even gathering the murky information may therefore be a lengthy process. Moreover, because lines are so broad, very high powers of radio-frequency radiation may be required to achieve saturation. Whereas solution pulse NMR uses transmitters of a few tens of watts, solid-state NMR may require transmitters rated at several hundreds of watts.

(a) The origins of linewidths in solids

There are two principal contributions to the linewidths of solids. One is the direct magnetic dipolar interaction between nuclear spins. As we saw in the discussion of spin–spin coupling, a nuclear magnetic moment will give rise to a local magnetic field, which points in different directions at different locations around the nucleus. If we are interested only in the component parallel to the direction of the applied magnetic field (because only this component has a significant effect), then we can use a classical expression to write the magnitude of the local magnetic field as

$$\mathcal{B}_{\text{loc}} = -\frac{\gamma\hbar\mu_0 m_I}{4\pi R^3}(1 - 3\cos^2\theta) \qquad (15.39)$$

Unlike in solution, this field is not motionally averaged to zero. Many nuclei may contribute to the total local field experienced by a nucleus of interest, and different nuclei in a sample may experience a wide range of fields. Typical dipole fields are of the order of 10^{-3} T, which corresponds to splittings and linewidths of the order of 10^4 Hz.

A second source of linewidth is the anisotropy of the chemical shift. We have seen that chemical shifts arise from the ability of the applied field to generate electron currents in molecules. In general, this ability depends on the orientation of the molecule relative to the applied field. In solution, when the molecule is tumbling rapidly, only the average value of the chemical shift is relevant. However, the anisotropy is not averaged to zero for stationary molecules in a solid, and molecules in different orientations have resonances at different frequencies. The chemical shift anisotropy also varies with the angle between the applied field and the principal axis of the molecule as $1 - 3\cos^2\theta$.

(b) The reduction of linewidths

Fortunately, there are techniques available for reducing the linewidths of solid samples. One technique, **magic-angle spinning** (MAS), takes note of the $1 - 3\cos^2\theta$ dependence of both the dipole–dipole interaction and the chemical shift anisotropy. The 'magic angle' is the angle at which $1 - 3\cos^2\theta = 0$, and corresponds to 54.74°. In the technique, the sample is spun at high speed at the magic angle to the applied field (Fig. 15.53). All the dipolar interactions and the anisotropies average to the value they would have at the magic angle, but at that angle they are zero. The difficulty with MAS is that the spinning frequency must not be less than the width of the spectrum, which is of the order of kilohertz. However, gas-driven sample spinners that can be rotated at up to 25 kHz are now routinely available, and a considerable body of work has been done.

Pulsed techniques similar to those described in the previous section may also be used to reduce linewidths. The dipolar field of protons, for instance, may be reduced by a decoupling procedure. However, because the range of coupling strengths is so large, radiofrequency power of the order of 1 kW is required. Elaborate pulse sequences have also been devised that reduce linewidths by averaging procedures that make use of twisting the magnetization vector through an elaborate series of angles.

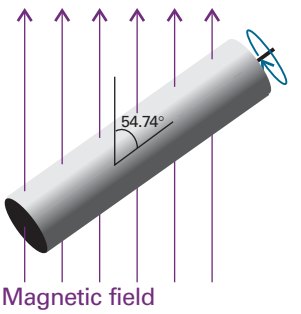

Fig. 15.53 In magic angle spinning, the sample spins at 54.74° (that is, $\arccos(\frac{1}{3})^{1/2}$) to the applied magnetic field. Rapid motion at this angle averages dipole–dipole interactions and chemical shift anisotropies to zero.

Electron paramagnetic resonance

Electron paramagnetic resonance (EPR) is less widely applicable than NMR because it cannot be detected in normal, spin-paired molecules and the sample must possess unpaired electron spins. It is used to study radicals formed during chemical reactions or by radiation, radicals that act as probes of biological structure, many *d*-metal complexes, and molecules in triplet states (such as those involved in phosphorescence, Section 14.3b). The sample may be a gas, a liquid, or a solid, but the free rotation of molecules in the gas phase gives rise to complications.

15.14 The EPR spectrometer

Both Fourier-transform (FT) and continuous wave (CW) EPR spectrometers are available. The FT-EPR instrument is based on the concepts developed in Section 15.8, except that pulses of microwaves are used to excite electron spins in the sample. The layout of the more common CW-EPR spectrometer is shown in Fig. 15.54. It consists

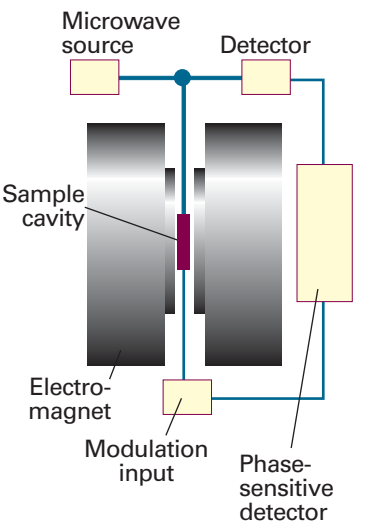

Fig. 15.54 The layout of a continuous-wave EPR spectrometer. A typical magnetic field is 0.3 T, which requires 9 GHz (3 cm) microwaves for resonance.

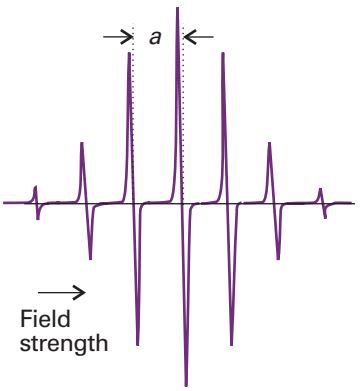

Fig. 15.55 The EPR spectrum of the benzene radical anion, $C_6H_6^-$, in fluid solution. *a* is the hyperfine splitting of the spectrum; the centre of the spectrum is determined by the *g*-value of the radical.

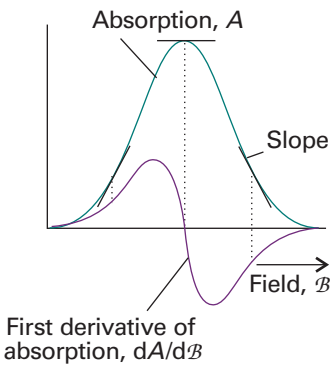

Fig. 15.56 When phase-sensitive detection is used, the signal is the first derivative of the absorption intensity. Note that the peak of the absorption corresponds to the point where the derivative passes through zero.

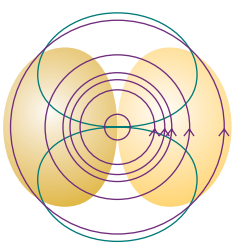

Fig. 15.57 An applied magnetic field can induce circulation of electrons that makes use of excited state orbitals (shown as a green outline).

of a microwave source (a klystron or a Gunn oscillator), a cavity in which the sample is inserted in a glass or quartz container, a microwave detector, and an electromagnet with a field that can be varied in the region of 0.3 T. The EPR spectrum is obtained by monitoring the microwave absorption as the field is changed, and a typical spectrum (of the benzene radical anion, $C_6H_6^-$) is shown in Fig. 15.55. The peculiar appearance of the spectrum, which is in fact the first-derivative of the absorption, arises from the detection technique, which is sensitive to the slope of the absorption curve (Fig. 15.56).

15.15 The *g*-value

Equation 15.13b gives the resonance frequency for a transition between the $m_s = -\frac{1}{2}$ and the $m_s = +\frac{1}{2}$ levels of a 'free' electron in terms of the *g*-value $g_e \approx 2.0023$. The magnetic moment of an unpaired electron in a radical also interacts with an external field, but the *g*-value is different from that for a free electron because of local magnetic fields induced by the molecular framework of the radical. Consequently, the resonance condition is normally written as

$$h\nu = g\mu_B\mathcal{B}_0 \tag{15.40}$$

where *g* is the ***g*-value** of the radical.

Illustration 15.4 *Calculating the g-value of an organic radical*

The centre of the EPR spectrum of the methyl radical occurred at 329.40 mT in a spectrometer operating at 9.2330 GHz (radiation belonging to the X band of the microwave region). Its *g*-value is therefore

$$g = \frac{h\nu}{\mu_B\mathcal{B}} = \frac{(6.626\,08\times10^{-34}\ \text{J s})\times(9.2330\times10^{9}\ \text{s}^{-1})}{(9.2740\times10^{-24}\ \text{J T}^{-1})\times(0.329\,40\ \text{T})} = 2.0027$$

Self-test 15.4 At what magnetic field would the methyl radical come into resonance in a spectrometer operating at 34.000 GHz (radiation belonging to the Q band of the microwave region)? [1.213 T]

The *g*-value in a molecular environment (a radical or a *d*-metal complex) is related to the ease with which the applied field can stir up currents through the molecular framework and the strength of the magnetic field the currents generate. Therefore, the *g*-value gives some information about electronic structure and plays a similar role in EPR to that played by shielding constants in NMR.

Electrons can migrate through the molecular framework by making use of excited states (Fig. 15.57). This additional path for circulation of electrons gives rise to a local magnetic field that adds to the applied field. Therefore, we expect that the ease of stirring up currents to be inversely proportional to the separation of energy levels, ΔE, in the molecule. As we saw in Section 10.8, the strength of the field generated by electronic currents in atoms (and analogously in molecules) is related to the extent of coupling between spin and orbital angular momenta. That is, the local field strength is proportional to the molecular spin–orbit coupling constant, ξ.

We can conclude from the discussion above that the *g*-value of a radical or *d*-metal complex differs from g_e, the 'free-electron' *g*-value, by an amount that is proportional to $\xi/\Delta E$. This proportionality is widely observed. Many organic radicals have *g*-values close to 2.0027 and inorganic radicals have *g*-values typically in the range 1.9 to 2.1. The *g*-values of paramagnetic *d*-metal complexes often differ considerably from g_e,

varying from 0 to 6, because in them ΔE is small (on account of the splitting of *d*-orbitals brought about by interactions with ligands, as we saw in Section 14.2).

Just as in the case of the chemical shift in NMR spectroscopy, the *g*-value is anisotropic: that is, its magnitude depends on the orientation of the radical with respect to the applied field. In solution, when the molecule is tumbling rapidly, only the average value of the *g*-value is observed. Therefore, anisotropy of the *g*-value is observed only for radicals trapped in solids.

15.16 Hyperfine structure

The most important feature of EPR spectra is their **hyperfine structure**, the splitting of individual resonance lines into components. In general in spectroscopy, the term 'hyperfine structure' means the structure of a spectrum that can be traced to interactions of the electrons with nuclei other than as a result of the latter's point electric charge. The source of the hyperfine structure in EPR is the magnetic interaction between the electron spin and the magnetic dipole moments of the nuclei present in the radical.

(a) The effects of nuclear spin

Consider the effect on the EPR spectrum of a single H nucleus located somewhere in a radical. The proton spin is a source of magnetic field, and depending on the orientation of the nuclear spin, the field it generates adds to or subtracts from the applied field. The total local field is therefore

$$\mathcal{B}_{\text{loc}} = \mathcal{B} + am_I \qquad m_I = \pm\tfrac{1}{2} \tag{15.41}$$

where a is the **hyperfine coupling constant**. Half the radicals in a sample have $m_I = +\frac{1}{2}$, so half resonate when the applied field satisfies the condition

$$h\nu = g\mu_{\text{B}}(\mathcal{B} + \tfrac{1}{2}a), \qquad \text{or} \qquad \mathcal{B} = \frac{h\nu}{g\mu_{\text{B}}} - \tfrac{1}{2}a \tag{15.42a}$$

The other half (which have $m_I = -\frac{1}{2}$) resonate when

$$h\nu = g\mu_{\text{B}}(\mathcal{B} - \tfrac{1}{2}a), \qquad \text{or} \qquad \mathcal{B} = \frac{h\nu}{g\mu_{\text{B}}} + \tfrac{1}{2}a \tag{15.42b}$$

Therefore, instead of a single line, the spectrum shows two lines of half the original intensity separated by a and centred on the field determined by g (Fig. 15.58).

If the radical contains an ^{14}N atom ($I = 1$), its EPR spectrum consists of three lines of equal intensity, because the ^{14}N nucleus has three possible spin orientations, and each spin orientation is possessed by one-third of all the radicals in the sample. In general, a spin-I nucleus splits the spectrum into $2I + 1$ hyperfine lines of equal intensity.

When there are several magnetic nuclei present in the radical, each one contributes to the hyperfine structure. In the case of equivalent protons (for example, the two CH_2 protons in the radical CH_3CH_2) some of the hyperfine lines are coincident. It is not hard to show that, if the radical contains N equivalent protons, then there are $N + 1$ hyperfine lines with a binomial intensity distribution (the intensity distribution given by Pascal's triangle). The spectrum of the benzene radical anion in Fig. 15.55, which has seven lines with intensity ratio 1:6:15:20:15:6:1, is consistent with a radical containing six equivalent protons. More generally, if the radical contains N equivalent nuclei with spin quantum number I, then there are $2NI + 1$ hyperfine lines with an intensity distribution based on a modified version of Pascal's triangle as shown in the following *Example*.

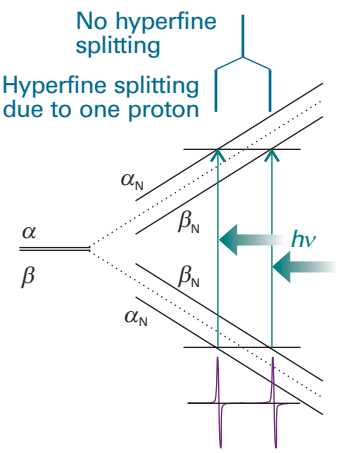

Fig. 15.58 The hyperfine interaction between an electron and a spin-$\frac{1}{2}$ nucleus results in four energy levels in place of the original two. As a result, the spectrum consists of two lines (of equal intensity) instead of one. The intensity distribution can be summarized by a simple stick diagram. The diagonal lines show the energies of the states as the applied field is increased, and resonance occurs when the separation of states matches the fixed energy of the microwave photon.

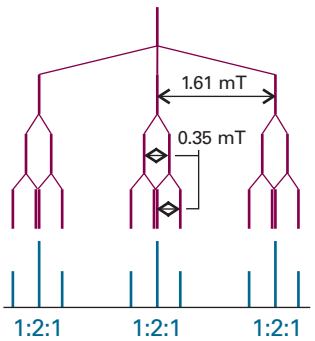

Fig. 15.59 The analysis of the hyperfine structure of radicals containing one ^{14}N nucleus ($I = 1$) and two equivalent protons.

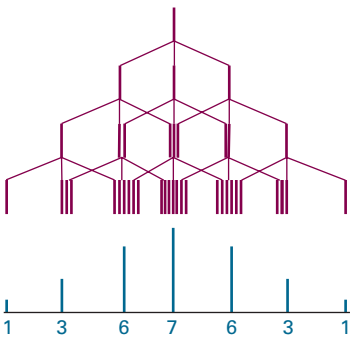

Fig. 15.60 The analysis of the hyperfine structure of radicals containing three equivalent ^{14}N nuclei.

Example 15.3 *Predicting the hyperfine structure of an EPR spectrum*

A radical contains one ^{14}N nucleus ($I = 1$) with hyperfine constant 1.61 mT and two equivalent protons ($I = \frac{1}{2}$) with hyperfine constant 0.35 mT. Predict the form of the EPR spectrum.

Method We should consider the hyperfine structure that arises from each type of nucleus or group of equivalent nuclei in succession. So, split a line with one nucleus, then each of those lines is split by a second nucleus (or group of nuclei), and so on. It is best to start with the nucleus with the largest hyperfine splitting; however, any choice could be made, and the order in which nuclei are considered does not affect the conclusion.

Answer The ^{14}N nucleus gives three hyperfine lines of equal intensity separated by 1.61 mT. Each line is split into doublets of spacing 0.35 mT by the first proton, and each line of these doublets is split into doublets with the same 0.35 mT splitting (Fig. 15.59). The central lines of each split doublet coincide, so the proton splitting gives 1:2:1 triplets of internal splitting 0.35 mT. Therefore, the spectrum consists of three equivalent 1:2:1 triplets.

Self-test 15.5 Predict the form of the EPR spectrum of a radical containing three equivalent ^{14}N nuclei. [Fig. 15.60]

The hyperfine structure of an EPR spectrum is a kind of fingerprint that helps to identify the radicals present in a sample. Moreover, because the magnitude of the splitting depends on the distribution of the unpaired electron near the magnetic nuclei present, the spectrum can be used to map the molecular orbital occupied by the unpaired electron. For example, because the hyperfine splitting in $C_6H_6^-$ is 0.375 mT, and one proton is close to a C atom with one-sixth the unpaired electron spin density (because the electron is spread uniformly around the ring), the hyperfine splitting caused by a proton in the electron spin entirely confined to a single adjacent C atom should be 6×0.375 mT = 2.25 mT. If in another aromatic radical we find a hyperfine splitting constant a, then the **spin density**, ρ, the probability that an unpaired electron is on the atom, can be calculated from the **McConnell equation**:

$$a = Q\rho \tag{15.43}$$

with $Q = 2.25$ mT. In this equation, ρ is the spin density on a C atom and a is the hyperfine splitting observed for the H atom to which it is attached.

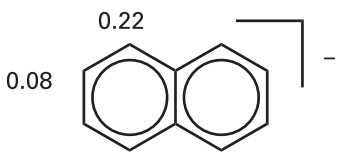

8

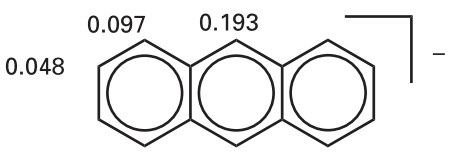

9

Illustration 15.5 *Using the McConnell equation*

The hyperfine structure of the EPR spectrum of the radical anion (naphthalene)$^-$ can be interpreted as arising from two groups of four equivalent protons. Those at the 1, 4, 5, and 8 positions in the ring have $a = 0.490$ mT and for those in the 2, 3, 6, and 7 positions have $a = 0.183$ mT. The densities obtained by using the McConnell equation are 0.22 and 0.08, respectively (**8**).

Self-test 15.6 The spin density in (anthracene)$^-$ is shown in (**9**). Predict the form of its EPR spectrum.

[A 1:2:1 triplet of splitting 0.43 mT split into a 1:4:6:4:1 quintet of splitting 0.22 mT, split into a 1:4:6:4:1 quintet of plitting 0.11 mT, $3 \times 5 \times 5 = 75$ lines in all]

(b) The origin of the hyperfine interaction

The hyperfine interaction is an interaction between the magnetic moments of the unpaired electron and the nuclei. There are two contributions to the interaction.

An electron in a *p* orbital does not approach the nucleus very closely, so it experiences a field that appears to arise from a point magnetic dipole. The resulting interaction is called the **dipole–dipole interaction**. The contribution of a magnetic nucleus to the local field experienced by the unpaired electron is given by an expression like that in eqn 15.28. A characteristic of this type of interaction is that it is anisotropic. Furthermore, just as in the case of NMR, the dipole–dipole interaction averages to zero when the radical is free to tumble. Therefore, hyperfine structure due to the dipole–dipole interaction is observed only for radicals trapped in solids.

An *s* electron is spherically distributed around a nucleus and so has zero average dipole–dipole interaction with the nucleus even in a solid sample. However, because an *s* electron has a nonzero probability of being at the nucleus, it is incorrect to treat the interaction as one between two point dipoles. An *s* electron has a Fermi contact interaction with the nucleus, which as we saw in Section 15.6d is a magnetic interaction that occurs when the point dipole approximation fails. The contact interaction is isotropic (that is, independent of the radical's orientation), and consequently is shown even by rapidly tumbling molecules in fluids (provided the spin density has some *s* character).

The dipole–dipole interactions of *p* electrons and the Fermi contact interaction of *s* electrons can be quite large. For example, a 2*p* electron in a nitrogen atom experiences an average field of about 3.4 mT from the ^{14}N nucleus. A 1*s* electron in a hydrogen atom experiences a field of about 50 mT as a result of its Fermi contact interaction with the central proton. More values are listed in Table 15.3. The magnitudes of the contact interactions in radicals can be interpreted in terms of the *s* orbital character of the molecular orbital occupied by the unpaired electron, and the dipole–dipole interaction can be interpreted in terms of the *p* character. The analysis of hyperfine structure therefore gives information about the composition of the orbital, and especially the hybridization of the atomic orbitals (see Problem 15.11).

We still have the source of the hyperfine structure of the $C_6H_6^-$ anion and other aromatic radical anions to explain. The sample is fluid, and as the radicals are tumbling the hyperfine structure cannot be due to the dipole–dipole interaction. Moreover, the protons lie in the nodal plane of the π orbital occupied by the unpaired electron, so the structure cannot be due to a Fermi contact interaction. The explanation lies in a **polarization mechanism** similar to the one responsible for spin–spin coupling in NMR. There is a magnetic interaction between a proton and the α electrons ($m_s = +\frac{1}{2}$) which results in one of the electrons tending to be found with a greater probability nearby (Fig. 15.61). The electron with opposite spin is therefore more likely to be close to the C atom at the other end of the bond. The unpaired electron on the C atom has a lower energy if it is parallel to that electron (Hund's rule favours parallel electrons on atoms), so the unpaired electron can detect the spin of the proton indirectly. Calculation using this model leads to a hyperfine interaction in agreement with the observed value of 2.25 mT.

Synoptic table 15.3* Hyperfine coupling constants for atoms, *a*/mT

Nuclide	Isotropic coupling	Anisotropic coupling
^{1}H	50.8 (1*s*)	
^{2}H	7.8 (1*s*)	
^{14}N	55.2 (2*s*)	3.4 (2*p*)
^{19}F	1720 (2*s*)	108.4 (2*p*)

* More values are given in the *Data section*.

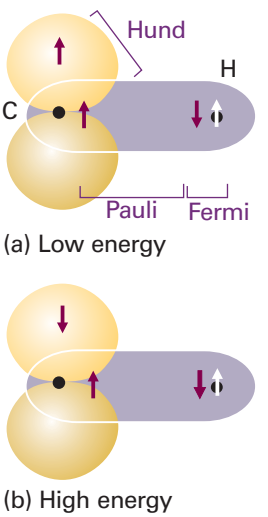

Fig. 15.61 The polarization mechanism for the hyperfine interaction in π-electron radicals. The arrangement in (a) is lower in energy than that in (b), so there is an effective coupling between the unpaired electron and the proton.

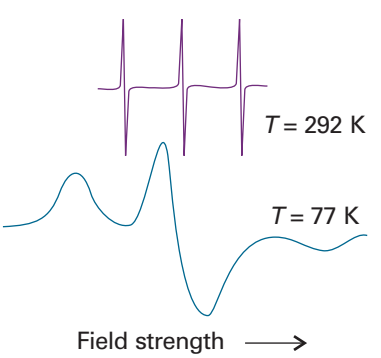

Fig. 15.62 ESR spectra of the di-*tert*-butyl nitroxide radical at 292 K (top) and 77 K (bottom). Adapted from J.R. Bolton, in *Biological applications of electron spin resonance*, H.M. Swartz, J.R. Bolton, and D.C. Borg (ed.), Wiley, New York (1972).

IMPACT ON BIOCHEMISTRY

I15.2 Spin probes

We saw in Sections 15.14 and 15.15 that anisotropy of the *g*-value and of the nuclear hyperfine interactions can be observed when a radical is immobilized in a solid. Figure 15.62 shows the variation of the lineshape of the EPR spectrum of the di-*tert*-butyl nitroxide radical (**10**) with temperature. At 292 K, the radical tumbles freely and isotropic hyperfine coupling to the ^{14}N nucleus gives rise to three sharp peaks. At 77 K,

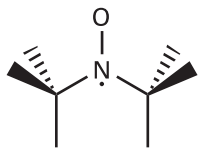

10

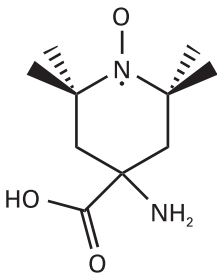

11

motion of the radical is restricted. Both isotropic and anisotropic hyperfine couplings determine the appearance of the spectrum, which now consists of three broad peaks.

A *spin probe* (or *spin label*) is a radical that interacts with a biopolymer and with an EPR spectrum that reports on the dynamical properties of the biopolymer. The ideal spin probe is one with a spectrum that broadens significantly as its motion is restricted to a relatively small extent. Nitroxide spin probes have been used to show that the hydrophobic interiors of biological membranes, once thought to be rigid, are in fact very fluid and individual lipid molecules move laterally through the sheet-like structure of the membrane.

Just as chemical exchange can broaden proton NMR spectra (Section 15.7), electron exchange between two radicals can broaden EPR spectra. Therefore, the distance between two spin probe molecules may be measured from the linewidths of their EPR spectra. The effect can be used in a number of biochemical studies. For example, the kinetics of association of two polypeptides labelled with the synthetic amino acid 2,2,6,6,-tetramethylpiperidine-1-oxyl-4-amino-4-carboxylic acid (**11**) may be studied by measuring the change in linewidth of the label with time. Alternatively, the thermodynamics of association may be studied by examining the temperature dependence of the linewidth.

Checklist of key ideas

- ☐ 1. The energy of an electron in a magnetic field $\mathcal{B}_0$ is $E_{m_s} = -g_e\gamma_e\hbar\mathcal{B}_0 m_s$, where γ_e is the magnetogyric ratio of the electron. The energy of a nucleus in a magnetic field $\mathcal{B}_0$ is $E_{m_I} = -\gamma\hbar\mathcal{B}_0 m_I$, where γ is the nuclear magnetogyric ratio.
- ☐ 2. The resonance condition for an electron in a magnetic field is $h\nu = g_e\mu_B\mathcal{B}_0$. The resonance condition for a nucleus in a magnetic field is $h\nu = \gamma\hbar\mathcal{B}_0$.
- ☐ 3. Nuclear magnetic resonance (NMR) is the observation of the frequency at which magnetic nuclei in molecules come into resonance with an electromagnetic field when the molecule is exposed to a strong magnetic field; NMR is a radiofrequency technique.
- ☐ 4. Electron paramagnetic resonance (EPR) is the observation of the frequency at which an electron spin comes into resonance with an electromagnetic field when the molecule is exposed to a strong magnetic field; EPR is a microwave technique.
- ☐ 5. The intensity of an NMR or EPR transition increases with the difference in population of α and β states and the strength of the applied magnetic field (as $\mathcal{B}_0^2$).
- ☐ 6. The chemical shift of a nucleus is the difference between its resonance frequency and that of a reference standard; chemical shifts are reported on the δ scale, in which $\delta = (\nu - \nu^\circ) \times 10^6/\nu^\circ$.
- ☐ 7. The observed shielding constant is the sum of a local contribution, a neighbouring group contribution, and a solvent contribution.
- ☐ 8. The fine structure of an NMR spectrum is the splitting of the groups of resonances into individual lines; the strength of the interaction is expressed in terms of the spin–spin coupling constant, J.
- ☐ 9. N equivalent spin-$\frac{1}{2}$ nuclei split the resonance of a nearby spin or group of equivalent spins into $N + 1$ lines with an intensity distribution given by Pascal's triangle.
- ☐ 10. Spin–spin coupling in molecules in solution can be explained in terms of the polarization mechanism, in which the interaction is transmitted through the bonds.
- ☐ 11. The Fermi contact interaction is a magnetic interaction that depends on the very close approach of an electron to the nucleus and can occur only if the electron occupies an s orbital.
- ☐ 12. Coalescence of the two lines occurs in conformational interchange or chemical exchange when the lifetime, τ, of the states is related to their resonance frequency difference, $\delta\nu$, by $\tau = 2^{1/2}/\pi\delta\nu$.
- ☐ 13. In Fourier-transform NMR, the spectrum is obtained by mathematical analysis of the free-induction decay of magnetization, the response of nuclear spins in a sample to the application of one or more pulses of radiofrequency radiation.
- ☐ 14. Spin relaxation is the nonradiative return of a spin system to an equilibrium distribution of populations in which the transverse spin orientations are random; the system returns exponentially to the equilibrium population distribution with a time constant called the spin–lattice relaxation time, T_1.
- ☐ 15. The spin–spin relaxation time, T_2, is the time constant for the exponential return of the system to random transverse spin orientations.
- ☐ 16. In proton decoupling of ^{13}C-NMR spectra, protons are made to undergo rapid spin reorientations and the ^{13}C nucleus

senses an average orientation. As a result, its resonance is a single line and not a group of lines.

☐ 17. The nuclear Overhauser effect (NOE) is the modification of one resonance by the saturation of another.

☐ 18. In two-dimensional NMR, spectra are displayed in two axes, with resonances belonging to different groups lying at different locations on the second axis. An example of a two-dimensional NMR technique is correlation spectroscopy (COSY), in which all spin–spin couplings in a molecule are determined. Another example is nuclear Overhauser effect spectroscopy (NOESY), in which internuclear distances up to about 0.5 nm are determined.

☐ 19. Magic-angle spinning (MAS) is technique in which the NMR linewidths in a solid sample are reduced by spinning at an angle of 54.74° to the applied magnetic field.

☐ 20. The EPR resonance condition is written $h\nu = g\mu_B\mathcal{B}$, where g is the g-value of the radical; the deviation of g from $g_e = 2.0023$ depends on the ability of the applied field to induce local electron currents in the radical.

☐ 21. The hyperfine structure of an EPR spectrum is its splitting of individual resonance lines into components by the magnetic interaction between the electron and nuclei with spin.

☐ 22. If a radical contains N equivalent nuclei with spin quantum number I, then there are $2NI + 1$ hyperfine lines with an intensity distribution given by a modified version of Pascal's triangle.

☐ 23. The hyperfine structure due to a hydrogen attached to an aromatic ring is converted to spin density, ρ, on the neighbouring carbon atom by using the McConnell equation: $a = Q\rho$ with $Q = 2.25$ mT.

Further reading

Articles and texts

N.M. Atherton, *Principles of electron spin resonance*. Ellis Horwood/Prentice Hall, Hemel Hempstead (1993).

E.D. Becker, *High resolution NMR: theory and chemical applications*. Academic Press, San Diego (2000).

R. Freeman, *Spin choreography: basic steps in high resolution NMR*. Oxford University Press (1998).

J.C. Lindon, G.E. Tranter, and J.L. Holmes (ed.), *Encyclopedia of spectroscopy and spectrometry*. Academic Press, San Diego (2000).

R.W. King and K.R. Williams. The Fourier transform in chemistry. Part 1. Nuclear magnetic resonance: Introduction. *J. Chem. Educ.* **66**, A213 (1989); Part 2. Nuclear magnetic resonance: The single pulse experiment. *Ibid*. A243; Part 3. Multiple-pulse experiments. *J. Chem. Educ.* **67**, A93 (1990); Part 4. NMR: Two-dimensional methods. *Ibid*. A125; A glossary of NMR terms. *Ibid*. A100.

M.T. Vlaardingerbroek and J.A. de Boer, *Magnetic resonance imaging: theory and practice*. Springer, Berlin (1999).

M.H. Levitt, *Spin dynamics*. Wiley (2001).

Sources of data and information

D.R. Lide (ed.), *CRC Handbook of Chemistry and Physics*, Section 9, CRC Press, Boca Raton (2000).

C.P. Poole, Jr. and H.A. Farach (ed.), *Handbook of electron spin resonance: data sources, computer technology, relaxation, and ENDOR*. Vols. 1–2. Springer, Berlin (1997, 1999).

Further information

Further information 15.1 *Fourier transformation of the FID curve*

The analysis of the FID curve is achieved by the standard mathematical technique of Fourier transformation, which we explored in the context of FT infrared spectroscopy (*Further information* 13.2). We start by noting that the signal $S(t)$ in the time domain, the total FID curve, is the sum (more precisely, the integral) over all the contributing frequencies

$$S(t) = \int_{-\infty}^{\infty} I(\nu) e^{-2\pi i \nu t} d\nu \qquad (15.44)$$

Because $e^{2\pi i \nu t} = \cos(2\pi\nu t) + i \sin(2\pi\nu t)$, the expression above is a sum over harmonically oscillating functions, with each one weighted by the intensity $I(\nu)$.

We need $I(\nu)$, the spectrum in the frequency domain; it is obtained by evaluating the integral

$$I(\nu) = 2\,\mathrm{Re} \int_0^{\infty} S(t) e^{2\pi i \nu t} dt \qquad (15.45)$$

where Re means take the real part of the following expression. This integral is very much like an overlap integral: it gives a nonzero value if $S(t)$ contains a component that matches the oscillating function $e^{2i\pi\nu t}$. The integration is carried out at a series of frequencies ν on a computer that is built into the spectrometer.

Discussion questions

15.1 Discuss in detail the origins of the local, neighbouring group, and solvent contributions to the shielding constant.

15.2 Discuss in detail the effects of a 90° pulse and of a 180° pulse on a system of spin-$\frac{1}{2}$ nuclei in a static magnetic field.

15.3 Suggest a reason why the relaxation times of ^{13}C nuclei are typically much longer than those of ^{1}H nuclei.

15.4 Discuss the origins of diagonal and cross peaks in the COSY spectrum of an AX system.

15.5 Discuss how the Fermi contact interaction and the polarization mechanism contribute to spin–spin couplings in NMR and hyperfine interactions in EPR.

15.6 Suggest how spin probes could be used to estimate the depth of a crevice in a biopolymer, such as the active site of an enzyme.

Exercises

15.1a What is the resonance frequency of a proton in a magnetic field of 14.1 T?

15.1b What is the resonance frequency of a ^{19}F nucleus in a magnetic field of 16.2 T?

15.2a ^{33}S has a nuclear spin of $\frac{3}{2}$ and a nuclear g-factor of 0.4289. Calculate the energies of the nuclear spin states in a magnetic field of 7.500 T.

15.2b ^{14}N has a nuclear spin of 1 and a nuclear g-factor of 0.404. Calculate the energies of the nuclear spin states in a magnetic field of 11.50 T.

15.3a Calculate the frequency separation of the nuclear spin levels of a ^{13}C nucleus in a magnetic field of 14.4 T given that the magnetogyric ratio is $6.73 \times 10^7\ T^{-1}\ s^{-1}$.

15.3b Calculate the frequency separation of the nuclear spin levels of a ^{14}N nucleus in a magnetic field of 15.4 T given that the magnetogyric ratio is $1.93 \times 10^7\ T^{-1}\ s^{-1}$.

15.4a In which of the following systems is the energy level separation the largest? (a) A proton in a 600 MHz NMR spectrometer, (b) a deuteron in the same spectrometer.

15.4b In which of the following systems is the energy level separation the largest? (a) A ^{14}N nucleus in (for protons) a 600 MHz NMR spectrometer, (b) an electron in a radical in a field of 0.300 T.

15.5a Calculate the energy difference between the lowest and highest nuclear spin states of a ^{14}N nucleus in a 15.00 T magnetic field.

15.5b Calculate the magnetic field needed to satisfy the resonance condition for unshielded protons in a 150.0 MHz radiofrequency field.

15.6a Use Table 15.2 to predict the magnetic fields at which (a) ^{1}H, (b) ^{2}H, (c) ^{13}C come into resonance at (i) 250 MHz, (ii) 500 MHz.

15.6b Use Table 15.2 to predict the magnetic fields at which (a) ^{14}N, (b) ^{19}F, and (c) ^{31}P come into resonance at (i) 300 MHz, (ii) 750 MHz.

15.7a Calculate the relative population differences ($\delta N/N$) for protons in fields of (a) 0.30 T, (b) 1.5 T, and (c) 10 T at 25°C.

15.7b Calculate the relative population differences ($\delta N/N$) for ^{13}C nuclei in fields of (a) 0.50 T, (b) 2.5 T, and (c) 15.5 T at 25°C.

15.8a The first generally available NMR spectrometers operated at a frequency of 60 MHz; today it is not uncommon to use a spectrometer that operates at 800 MHz. What are the relative population differences of ^{13}C spin states in these two spectrometers at 25°C?

15.8b What are the relative values of the chemical shifts observed for nuclei in the spectrometers mentioned in Exercise 15.8a in terms of (a) δ values, (b) frequencies?

15.9a The chemical shift of the CH_3 protons in acetaldehyde (ethanal) is $\delta = 2.20$ and that of the CHO proton is 9.80. What is the difference in local magnetic field between the two regions of the molecule when the applied field is (a) 1.5 T, (b) 15 T?

15.9b The chemical shift of the CH_3 protons in diethyl ether is $\delta = 1.16$ and that of the CH_2 protons is 3.36. What is the difference in local magnetic field between the two regions of the molecule when the applied field is (a) 1.9 T, (b) 16.5 T?

15.10a Sketch the appearance of the ^{1}H-NMR spectrum of acetaldehyde (ethanal) using $J = 2.90$ Hz and the data in Exercise 15.9a in a spectrometer operating at (a) 250 MHz, (b) 500 MHz.

15.10b Sketch the appearance of the ^{1}H-NMR spectrum of diethyl ether using $J = 6.97$ Hz and the data in Exercise 15.9b in a spectrometer operating at (a) 350 MHz, (b) 650 MHz.

15.11a Two groups of protons are made equivalent by the isomerization of a fluxional molecule. At low temperatures, where the interconversion is slow, one group has $\delta = 4.0$ and the other has $\delta = 5.2$. At what rate of interconversion will the two signals merge in a spectrometer operating at 250 MHz?

15.11b Two groups of protons are made equivalent by the isomerization of a fluxional molecule. At low temperatures, where the interconversion is slow, one group has $\delta = 5.5$ and the other has $\delta = 6.8$. At what rate of interconversion will the two signals merge in a spectrometer operating at 350 MHz?

15.12a Sketch the form of the ^{19}F-NMR spectra of a natural sample of tetrafluoroborate ions, BF_4^-, allowing for the relative abundances of $^{10}BF_4^-$ and $^{11}BF_4^-$.

15.12b From the data in Table 15.2, predict the frequency needed for ^{31}P-NMR in an NMR spectrometer designed to observe proton resonance at 500 MHz. Sketch the proton and ^{31}P resonances in the NMR spectrum of PH_4^+.

15.13a Sketch the form of an $A_3M_2X_4$ spectrum, where A, M, and X are protons with distinctly different chemical shifts and $J_{AM} > J_{AX} > J_{MX}$.

15.13b Sketch the form of an $A_2M_2X_5$ spectrum, where A, M, and X are protons with distinctly different chemical shifts and $J_{AM} > J_{AX} > J_{MX}$.

15.14a Which of the following molecules have sets of nuclei that are chemically but not magnetically equivalent? (a) CH_3CH_3, (b) $CH_2{=}CH_2$.

15.14b Which of the following molecules have sets of nuclei that are chemically but not magnetically equivalent? (a) $CH_2{=}C{=}CF_2$, (b) *cis*- and *trans*-$[Mo(CO)_4(PH_3)_2]$.

15.15a The duration of a 90° or 180° pulse depends on the strength of the $\mathcal{B}_1$ field. If a 90° pulse requires 10 μs, what is the strength of the $\mathcal{B}_1$ field? How long would the corresponding 180° pulse require?

15.15b The duration of a 90° or 180° pulse depends on the strength of the $\mathcal{B}_1$ field. If a 180° pulse requires 12.5 μs, what is the strength of the $\mathcal{B}_1$ field? How long would the corresponding 90° pulse require?

15.16a What magnetic field would be required in order to use an EPR X–band spectrometer (9 GHz) to observe ^{1}H-NMR and a 300 MHz spectrometer to observe EPR?

15.16b Some commercial EPR spectrometers use 8 mm microwave radiation (the Q band). What magnetic field is needed to satisfy the resonance condition?

15.17a The centre of the EPR spectrum of atomic hydrogen lies at 329.12 mT in a spectrometer operating at 9.2231 GHz. What is the *g*-value of the electron in the atom?

15.17b The centre of the EPR spectrum of atomic deuterium lies at 330.02 mT in a spectrometer operating at 9.2482 GHz. What is the *g*-value of the electron in the atom?

15.18a A radical containing two equivalent protons shows a three-line spectrum with an intensity distribution 1:2:1. The lines occur at 330.2 mT, 332.5 mT, and 334.8 mT. What is the hyperfine coupling constant for each proton? What is the *g*-value of the radical given that the spectrometer is operating at 9.319 GHz?

15.18b A radical containing three equivalent protons shows a four–line spectrum with an intensity distribution 1:3:3:1. The lines occur at 331.4 mT, 333.6 mT, 335.8 mT, and 338.0 mT. What is the hyperfine coupling constant for each proton? What is the *g*-value of the radical given that the spectrometer is operating at 9.332 GHz?

15.19a A radical containing two inequivalent protons with hyperfine constants 2.0 mT and 2.6 mT gives a spectrum centred on 332.5 mT. At what fields do the hyperfine lines occur and what are their relative intensities?

15.19b A radical containing three inequivalent protons with hyperfine constants 2.11 mT, 2.87 mT, and 2.89 mT gives a spectrum centred on 332.8 mT. At what fields do the hyperfine lines occur and what are their relative intensities?

15.20a Predict the intensity distribution in the hyperfine lines of the EPR spectra of (a) $\cdot CH_3$, (b) $\cdot CD_3$.

15.20b Predict the intensity distribution in the hyperfine lines of the EPR spectra of (a) $\cdot CH_2H_3$, (b) $\cdot CD_2CD_3$.

15.21a The benzene radical anion has $g = 2.0025$. At what field should you search for resonance in a spectrometer operating at (a) 9.302 GHz, (b) 33.67 GHz?

15.21b The naphthalene radical anion has $g = 2.0024$. At what field should you search for resonance in a spectrometer operating at (a) 9.312 GHz, (b) 33.88 GHz?

15.22a The EPR spectrum of a radical with a single magnetic nucleus is split into four lines of equal intensity. What is the nuclear spin of the nucleus?

15.22b The EPR spectrum of a radical with two equivalent nuclei of a particular kind is split into five lines of intensity ratio 1:2:3:2:1. What is the spin of the nuclei?

15.23a Sketch the form of the hyperfine structures of radicals XH_2 and XD_2, where the nucleus X has $I = \frac{5}{2}$.

15.23b Sketch the form of the hyperfine structures of radicals XH_3 and XD_3, where the nucleus X has $I = \frac{3}{2}$.

Problems*

Numerical problems

15.1 A scientist investigates the possibility of neutron spin resonance, and has available a commercial NMR spectrometer operating at 300 MHz. What field is required for resonance? What is the relative population difference at room temperature? Which is the lower energy spin state of the neutron?

15.2 Two groups of protons have $\delta = 4.0$ and $\delta = 5.2$ and are interconverted by a conformational change of a fluxional molecule. In a 60 MHz spectrometer the spectrum collapsed into a single line at 280 K but at 300 MHz the collapse did not occur until the temperature had been raised to 300 K. What is the activation energy of the interconversion?

15.3‡ Suppose that the FID in Fig. 15.31 was recorded in a 300 MHz spectrometer, and that the interval between maxima in the oscillations in the FID is 0.10 s. What is the Larmor frequency of the nuclei and the spin–spin relaxation time?

15.4‡ In a classic study of the application of NMR to the measurement of rotational barriers in molecules, P.M. Nair and J.D. Roberts (*J. Am. Chem. Soc.* **79**, 4565 (1957)) obtained the 40 MHz ^{19}F-NMR spectrum of $F_2BrCCBrCl_2$. Their spectra are reproduced in Fig. 15.63. At 193 K the spectrum shows five resonance peaks. Peaks I and III are separated by 160 Hz, as are IV and V. The ratio of the integrated intensities of peak II to peaks I, III, IV, and V is approximately 10 to 1. At 273 K, the five peaks have collapsed into

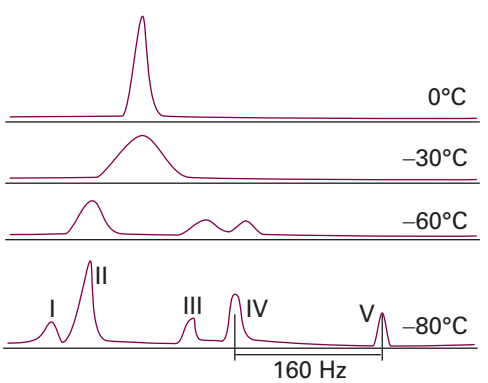

Fig. 15.63

* Problems denoted with the symbol ‡ were supplied by Charles Trapp and Carmen Giunta.

one. Explain the spectrum and its change with temperature. At what rate of interconversion will the spectrum collapse to a single line? Calculate the rotational energy barrier between the rotational isomers on the assumption that it is related to the rate of interconversion between the isomers.

15.5‡ Various versions of the Karplus equation (eqn 15.27) have been used to correlate data on vicinal proton coupling constants in systems of the type $R_1R_2CHCHR_3R_4$. The original version, (M. Karplus, *J. Am. Chem. Soc.* **85**, 2870 (1963)), is ${}^3J_{HH} = A\cos^2\phi_{HH} + B$. When $R_3 = R_4 = H$, ${}^3J_{HH} = 7.3$ Hz; when $R_3 = CH_3$ and $R_4 = H$, ${}^3J_{HH} = 8.0$ Hz; when $R_3 = R_4 = CH_3$, ${}^3J_{HH} = 11.2$ Hz. Assume that only staggered conformations are important and determine which version of the Karplus equation fits the data better.

15.6‡ It might be unexpected that the Karplus equation, which was first derived for ${}^3J_{HH}$ coupling constants, should also apply to vicinal coupling between the nuclei of metals such as tin. T.N. Mitchell and B. Kowall (*Magn. Reson. Chem.* **33**, 325 (1995)) have studied the relation between ${}^3J_{HH}$ and ${}^3J_{SnSn}$ in compounds of the type $Me_3SnCH_2CHRSnMe_3$ and find that ${}^3J_{SnSn} = 78.86{}^3J_{HH} + 27.84$ Hz. (a) Does this result support a Karplus type equation for tin? Explain your reasoning. (b) Obtain the Karplus equation for ${}^3J_{SnSn}$ and plot it as a function of the dihedral angle. (c) Draw the preferred conformation.

15.7 Figure 15.64 shows the proton COSY spectrum of 1-nitropropane. Account for the appearance of off-diagonal peaks in the spectrum.

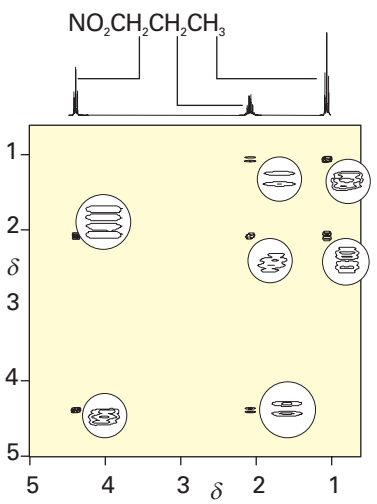

Fig. 15.64 The COSY spectrum of 1-nitropropane ($NO_2CH_2CH_2CH_3$). The circles show enhanced views of the spectral features. (Spectrum provided by Prof. G. Morris.)

15.8 The angular NO_2 molecule has a single unpaired electron and can be trapped in a solid matrix or prepared inside a nitrite crystal by radiation damage of NO_2^- ions. When the applied field is parallel to the OO direction the centre of the spectrum lies at 333.64 mT in a spectrometer operating at 9.302 GHz. When the field lies along the bisector of the ONO angle, the resonance lies at 331.94 mT. What are the *g*-values in the two orientations?

15.9 The hyperfine coupling constant in $\cdot CH_3$ is 2.3 mT. Use the information in Table 15.3 to predict the splitting between the hyperfine lines of the spectrum of $\cdot CD_3$. What are the overall widths of the hyperfine spectra in each case?

15.10 The *p*-dinitrobenzene radical anion can be prepared by reduction of *p*-dinitrobenzene. The radical anion has two equivalent N nuclei ($I = 1$) and four equivalent protons. Predict the form of the EPR spectrum using $a(N) = 0.148$ mT and $a(H) = 0.112$ mT.

15.11 When an electron occupies a 2*s* orbital on an N atom it has a hyperfine interaction of 55.2 mT with the nucleus. The spectrum of NO_2 shows an isotropic hyperfine interaction of 5.7 mT. For what proportion of its time is the unpaired electron of NO_2 occupying a 2*s* orbital? The hyperfine coupling constant for an electron in a 2*p* orbital of an N atom is 3.4 mT. In NO_2 the anisotropic part of the hyperfine coupling is 1.3 mT. What proportion of its time does the unpaired electron spend in the 2*p* orbital of the N atom in NO_2? What is the total probability that the electron will be found on (a) the N atoms, (b) the O atoms? What is the hybridization ratio of the N atom? Does the hybridization support the view that NO_2 is angular?

15.12 The hyperfine coupling constants observed in the radical anions (**12**), (**13**), and (**14**) are shown (in millitesla, mT). Use the value for the benzene radical anion to map the probability of finding the unpaired electron in the π orbital on each C atom.

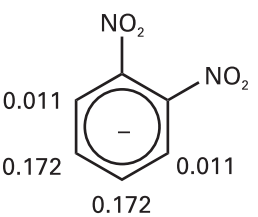

12

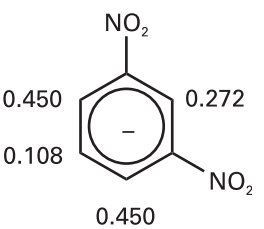

13

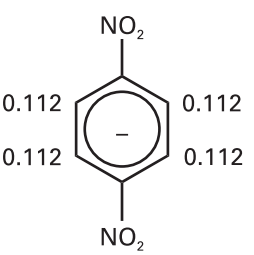

14

Theoretical problems

15.13 Calculate σ_d for a hydrogenic atom with atomic number *Z*.

15.14 In this problem you will use the molecular electronic structure methods described in Chapter 11 to investigate the hypothesis that the magnitude of the ^{13}C chemical shift correlates with the net charge on a ^{13}C atom. (a) Using molecular modelling software[3] and the computational method of your choice, calculate the net charge at the C atom *para* to the substituents in this series of molecules: benzene, phenol, toluene, trifluorotoluene, benzonitrile, and nitrobenzene. (b) The ^{13}C chemical shifts of the *para* C atoms in each of the molecules that you examined in part (a) are given below:

Substituent	OH	CH_3	H	CF_3	CN	NO_2
δ	130.1	128.4	128.5	128.9	129.1	129.4

Is there a linear correlation between net charge and ^{13}C chemical shift of the *para* C atom in this series of molecules? (c) If you did find a correlation in part (b), use the concepts developed in this chapter to explain the physical origins of the correlation.

[3] The web site contains links to molecular modelling freeware and to other sites where you may perform molecular orbital calculations directly from your web browser.

15.15 The z-component of the magnetic field at a distance R from a magnetic moment parallel to the z-axis is given by eqn 15.28. In a solid, a proton at a distance R from another can experience such a field and the measurement of the splitting it causes in the spectrum can be used to calculate R. In gypsum, for instance, the splitting in the H_2O resonance can be interpreted in terms of a magnetic field of 0.715 mT generated by one proton and experienced by the other. What is the separation of the protons in the H_2O molecule?

15.16 In a liquid, the dipolar magnetic field averages to zero: show this result by evaluating the average of the field given in eqn 15.28. *Hint*. The volume element is $\sin\theta\,\mathrm{d}\theta\mathrm{d}\phi$ in polar coordinates.

15.17 The shape of a spectral line, $I(\omega)$, is related to the free induction decay signal $G(t)$ by

$$I(\omega) = a\,\mathrm{Re}\int_0^\infty G(t)\mathrm{e}^{\mathrm{i}\omega t}\mathrm{d}t$$

where a is a constant and 'Re' means take the real part of what follows. Calculate the lineshape corresponding to an oscillating, decaying function $G(t) = \cos\omega_0 t\,\mathrm{e}^{-t/\tau}$.

15.18 In the language of Problem 15.17, show that, if $G(t) = (a\cos\omega_1 t + b\cos\omega_2 t)\mathrm{e}^{-t/\tau}$, then the spectrum consists of two lines with intensities proportional to a and b and located at $\omega = \omega_1$ and ω_2, respectively.

15.19 EPR spectra are commonly discussed in terms of the parameters that occur in the *spin-hamiltonian*, a hamiltonian operator that incorporates various effects involving spatial operators (like the orbital angular momentum) into operators that depend on the spin alone. Show that, if you use $H = -g_e\gamma_e\mathcal{B}_0 s_z - \gamma_e\mathcal{B}_0 I_z$ as the true hamiltonian, then from second-order perturbation theory (and specifically eqn 9.65), the eigenvalues of the spin are the same as those of the spin-hamiltonian $H_{\mathrm{spin}} = -g\gamma_e\mathcal{B}_0 s_z$ (note the g in place of g_e) and find an expression for g.

Applications: to biochemistry and medicine

15.20 Interpret the following features of the NMR spectra of hen lysozyme: (a) saturation of a proton resonance assigned to the side chain of methionine-105 changes the intensities of proton resonances assigned to the side chains of tryptophan-28 and tyrosine-23; (b) saturation of proton resonances assigned to tryptophan-28 did not affect the spectrum of tyrosine-23.

15.21 When interacting with a large biopolymer or even larger organelle, a small molecule might not rotate freely in all directions and the dipolar interaction might not average to zero. Suppose a molecule is bound so that, although the vector separating two protons may rotate freely around the z-axis, the colatitude may vary only between 0 and θ'. Average the dipolar field over this restricted range of orientations and confirm that the average vanishes when $\theta' = \pi$ (corresponding to rotation over an entire sphere). What is the average value of the local dipolar field for the H_2O molecule in Problem 15.15 if it is bound to a biopolymer that enables it to rotate up to $\theta' = 30°$?

15.22 Suggest a reason why the spin–lattice relaxation time of benzene (a small molecule) in a mobile, deuterated hydrocarbon solvent increases with temperature whereas that of an oligonucleotide (a large molecule) decreases.

15.23 NMR spectroscopy may be used to determine the equilibrium constant for dissociation of a complex between a small molecule, such as an enzyme inhibitor I, and a protein, such as an enzyme E:

$$\mathrm{EI} \rightleftharpoons \mathrm{E} + \mathrm{I} \qquad K_\mathrm{I} = [\mathrm{E}][\mathrm{I}]/[\mathrm{EI}]$$

In the limit of slow chemical exchange, the NMR spectrum of a proton in I would consist of two resonances: one at ν_I for free I and another at ν_EI for bound I. When chemical exchange is fast, the NMR spectrum of the same proton in I consists of a single peak with a resonance frequency ν given by $\nu = f_\mathrm{I}\nu_\mathrm{I} + f_\mathrm{EI}\nu_\mathrm{EI}$, where $f_\mathrm{I} = [\mathrm{I}]/([\mathrm{I}] + [\mathrm{EI}])$ and $f_\mathrm{EI} = [\mathrm{EI}]/([\mathrm{I}] + [\mathrm{EI}])$ are, respectively, the fractions of free I and bound I. For the purposes of analysing the data, it is also useful to define the frequency differences $\delta\nu = \nu - \nu_\mathrm{I}$ and $\Delta\nu = \nu_\mathrm{EI} - \nu_\mathrm{I}$. Show that, when the initial concentration of I, $[\mathrm{I}]_0$, is much greater than the initial concentration of E, $[\mathrm{E}]_0$, a plot of $[\mathrm{I}]_0$ against $\delta\nu^{-1}$ is a straight line with slope $[\mathrm{E}]_0\Delta\nu$ and y-intercept $-K_\mathrm{I}$.

15.24 The molecular electronic structure methods described in Chapter 11 may be used to predict the spin density distribution in a radical. Recent EPR studies have shown that the amino acid tyrosine participates in a number of biological electron transfer reactions, including the processes of water oxidation to O_2 in plant photosystem II and of O_2 reduction to water in cytochrome c oxidase (*Impact I17.2*). During the course of these electron transfer reactions, a tyrosine radical forms, with spin density delocalized over the side chain of the amino acid. (a) The phenoxy radical shown in (**15**) is a suitable model of the tyrosine radical. Using molecular modelling software and the computational method of your choice (semi-empirical or *ab initio* methods), calculate the spin densities at the O atom and at all of the C atoms in (**15**). (b) Predict the form of the EPR spectrum of (**15**).

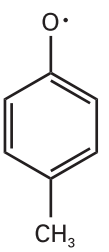

15

15.25 Sketch the EPR spectra of the di-*tert*-butyl nitroxide radical (**10**) at 292 K in the limits of very low concentration (at which electron exchange is negligible), moderate concentration (at which electron exchange effects begin to be observed), and high concentration (at which electron exchange effects predominate). Discuss how the observation of electron exchange between nitroxide spin probes can inform the study of lateral mobility of lipids in a biological membrane.

15.26 You are designing an MRI spectrometer. What field gradient (in microtesla per metre, $\mu\mathrm{T\,m^{-1}}$) is required to produce a separation of 100 Hz between two protons separated by the long diameter of a human kidney (taken as 8 cm) given that they are in environments with $\delta = 3.4$? The radiofrequency field of the spectrometer is at 400 MHz and the applied field is 9.4 T.

15.27 Suppose a uniform disk-shaped organ is in a linear field gradient, and that the MRI signal is proportional to the number of protons in a slice of width δx at each horizontal distance x from the centre of the disk. Sketch the shape of the absorption intensity for the MRI image of the disk before any computer manipulation has been carried out.